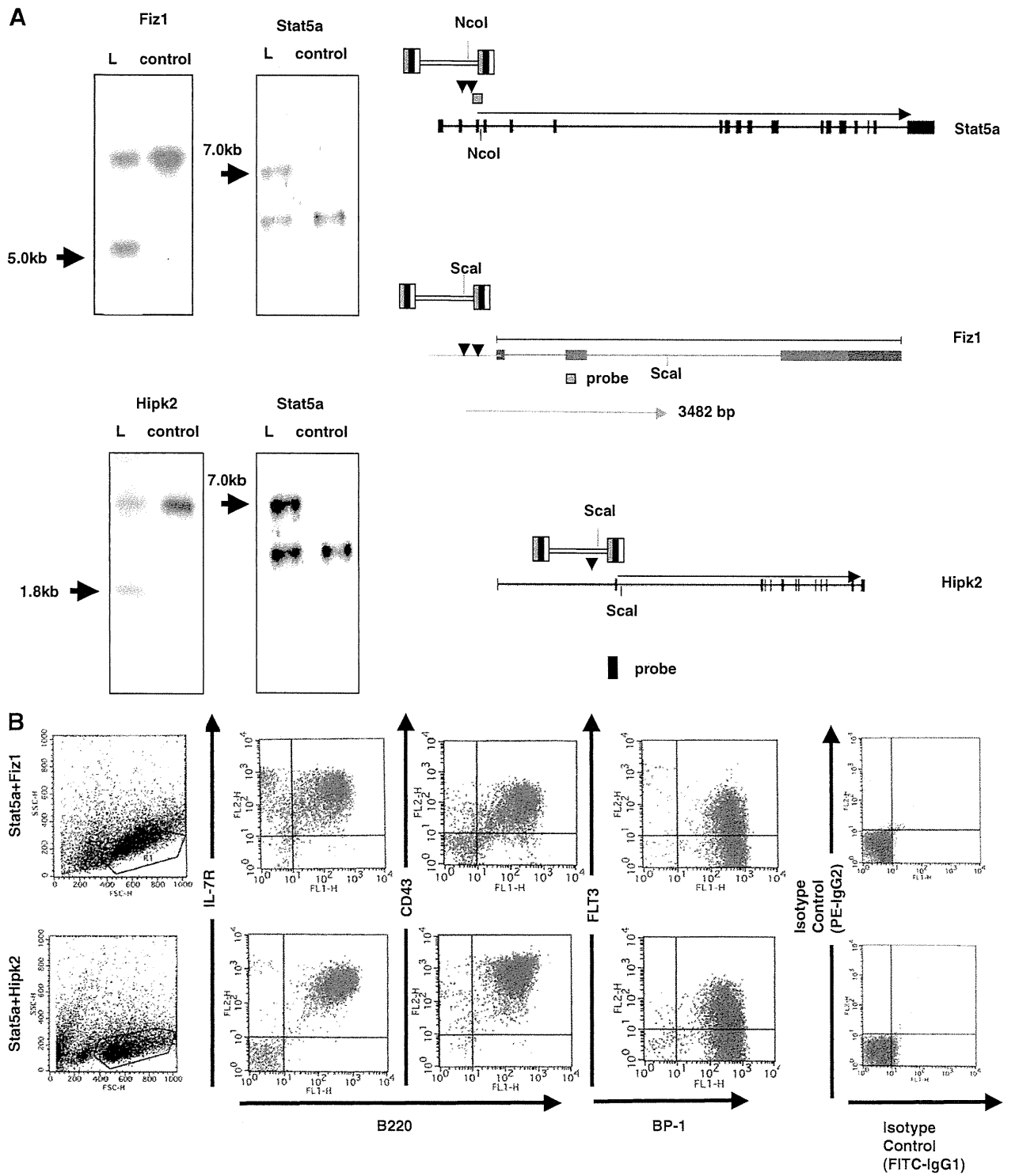

Figure 1. Clonality of B-LBL cells with dual integration. (A) Southern hybridization of LBL cells with *Stat5a* and *Fiz1* or *Stat5a* and *Hipk2* integration. The right scheme shows *NcoI* and *ScaI* sites within the MLV genome and immediately near the third exon of the *Stat5a* gene. The fragments of MLV-mouse genome DNA were visualized on the blot (indicated by arrows), and in these blots, the intensity of the fragments from provirus-integrated *Fiz1* and *Hipk2* was nearly identical to that of fragments from the nonintegrated allele. (B) Flow cytometry analysis of B-LBL cells with dual integration into *Stat5a* and *Fiz1* or *Stat5a* and *Hipk2*. FL2-H, Fluorescence 2-height. *(continued on next page)*

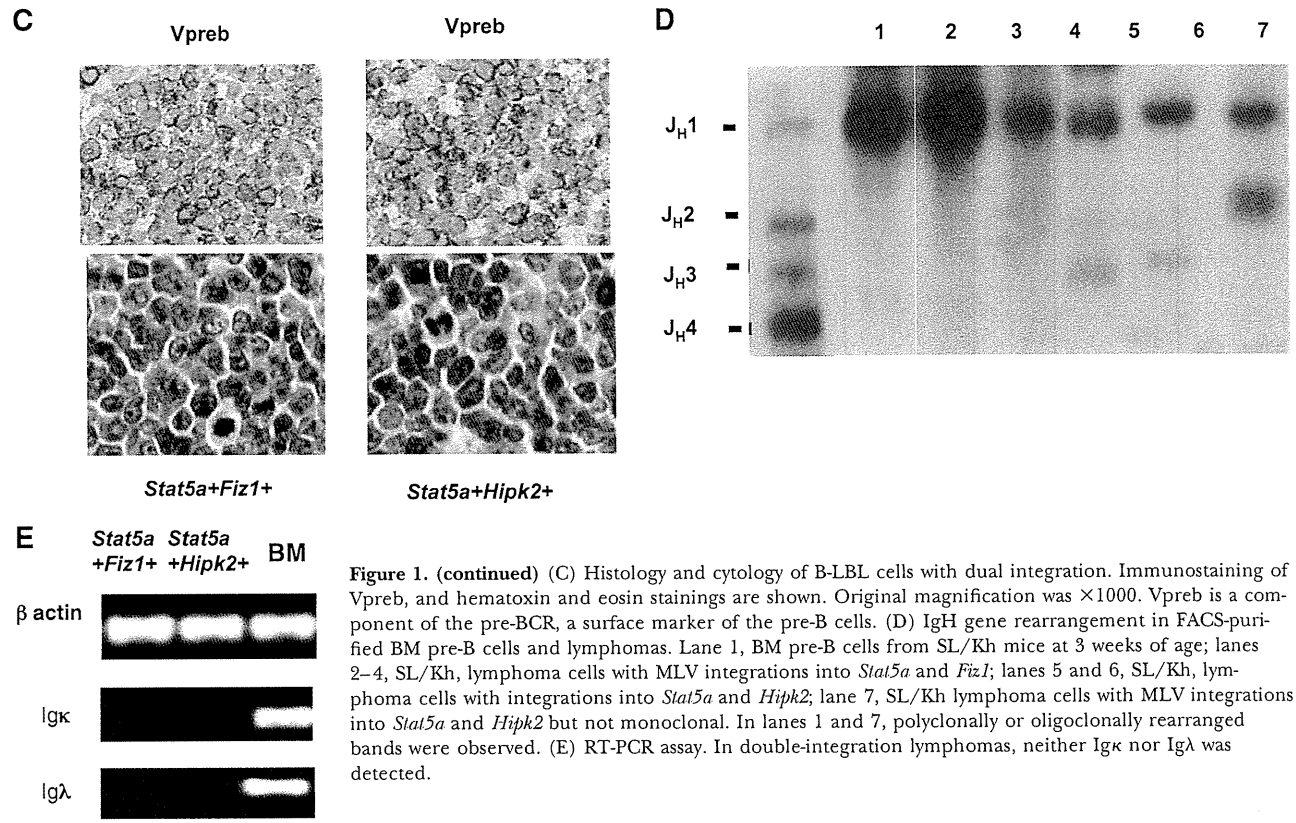

Figure 1. (continued) (C) Histology and cytology of B-LBL cells with dual integration. Immunostaining of Vpreb, and hematoxin and eosin stainings are shown. Original magnification was ×1000. Vpreb is a component of the pre-BCR, a surface marker of the pre-B cells. (D) IgH gene rearrangement in FACS-purified BM pre-B cells and lymphomas. Lane 1, BM pre-B cells from SL/Kh mice at 3 weeks of age; lanes 2–4, SL/Kh, lymphoma cells with MLV integrations into *Stat5a* and *Fiz1*; lanes 5 and 6, SL/Kh, lymphoma cells with integrations into *Stat5a* and *Hipk2*; lane 7, SL/Kh lymphoma cells with MLV integrations into *Stat5a* and *Hipk2* but not monoclonal. In lanes 1 and 7, polyclonally or oligoclonally rearranged bands were observed. (E) RT-PCR assay. In double-integration lymphomas, neither Igκ nor Igλ was detected.

sequences were: 5B4, 5′-GAGGGCTTGGACCTCTCGTCTCCTA-AAAAACCACG-3′, and 5F1, 5′-GTCTCTCCCAAACTCTCCCCCTCTC-CAACC-3′, in the first step and 5F2, 5′-CCTCCTCTGACGGAGATGGC-GACAGAGAAGAGG-3′, and 5B1, 5′-GAGGGCTTGGACCTCTCGTCTC-CTAAAAGAACCACG-3′, in the second step of cycles for nested PCR. Sequence analysis of the amplification products was performed with a Thermosequenase kit (GE Healthcare, Buckinghamshire, UK).

Southern blot of lymphoma DNA

The detailed protocol for detection of provirus integration into the host gene has been reported previously [9]. In brief, lymphoma DNA was digested with *Nco*I and *Sca*I (New England Biolabs, Ipswich, MA, USA). Probes for *Fiz1* and *Hipk2* were synthesized by PCR from the genomic DNA of SL/Kh mice and labeled with the Megaprime DNA-labeling system (GE Healthcare). The sequences were: 5′-CTTCCGTCATGGAAGACTCC-3′ and 5′-AGCAGGCCAGTG-GAGTCTCG-3′ for *Fiz 1* (exon 2) and 5′-TACCTTACGAGCAGACCATC-3′ and 5′-CAAAGACTAAGCACGTGTGG-3′ for *Hipk2* (exon 2). When the integration was completely clonal, the density ratio of the digested fragment, including MLV and the host gene DNA from the integrated allele, to the native *Stat5a* gene from the intact allele was nearly 1.0.

Colony growth assay

Prior to stimulation, lymphoma cells were grown for 6 h in RPMI. Lymphoma cells were washed once with PBS. After washing, they were suspended in 10 ml of a semi-solid medium.

Methocult (Stemcell Technologies, Vancouver, Canada), containing IL-7, was used as a basic semisolid medium in the colony assay. To detect early growth before 48 h, we defined the colony as a cluster of greater than five cells but after 48 h, only those of >20 cells. The cells were incubated in the medium with 10% FCS, 50 mM β-ME, and 100 mg/ml penicillin-streptomycin. Cultures were established in a humidified atmosphere at 37°C with 5% CO_2.

Ig gene recombination in the genome of lymphoma tissue

We confirmed the clonality by detection of a single IgH D_H-J_H recombination [8]. In brief, the lymphoma genomic DNA was subjected to PCR with primers designed to amplify four possible junctions between the D-Q52 and J_H regions. The primers for the first round were: 5′-CACAGAGAATTCTCCATAGTTGAT-AGCTCAG-3′ (D_HQ52-1; sense) and 5′-AGGCTCTGAGATCCCTAGACAG-3′ (J_H4-1; antisense). PCR conditions were as follows: denaturation for 1 min at 95°C, annealing for 1 min at 60°C, and extension for 2.5 min at 72°C (28 cycles). Two microliters of each reaction was subjected to a second round of PCR using a pair of internal primers: 5′-GCCTCAGAATTCCTGTGGTCTCT-GACTGGT-3′ (D_HQ52-2; sense) and 5′-GGGTCTAGACTCTCAGCCGGCTC-CCTCAGGG-3′ (J_H4-2; antisense). PCR was repeated as above. The PCR products were electrophoresed in an agarose gel, blotted onto a nylon membrane (GE Healthcare), and probed with a J_H4 probe for confirmation of the clonality of the cells by detection of IgH rearrangement [20]. RT-PCR assay for IgL will be described below. IgH J_H probe was the *Eco*RI-*Hin*dIII fragment encoding J_H4 [5, 24].

Flow cytometry

We used a protocol that has been described previously [8]. In brief, a single-cell suspension was prepared from femur BM plugs and axillary lymphoma tissue. The cell density was adjusted to 106 cells/ml, and the cells were analyzed in a FACScan apparatus (Becton Dickinson, Mountain View, CA, USA). The following antibodies were purchased commercially: FITC-labeled anti-BP-1 (clone 6C3), PE-labeled anti-B220 (clone RA3-6B2), anti-IL-7R (clone A7R34), and anti-CD24 (clone 30-F1;

eBioscience, San Diego, CA, USA) and anti-CD43 (clone S7), FITC-anti mouse IgG1, and PE-anti mouse IgG2 (BD Biosciences, San Diego, CA, USA). We stained BM early B cells and their fate in SL/Kh, NFS.SL/Kh-Bombl, and NFS. It was contained with 1:10,000-diluted mAb for 15 min.

Western blots and immunohistochemistry

The extract of sorted BP-1$^+$ B220$^+$ pre-B cells from the SL/Kh BM were used as a control. Antibodies to Fiz1 (sc-101955), Flt3 (sc-1496-1), Hipk2 (sc-10294), and Vpreb (sc-33128) were purchased from Santa Cruz Biotechnology (Santa Cruz, CA, USA). The Western blotting protocol has been described previously [5]. Phospho-specific antibodies against STAT5A (Tyr694) were obtained from Cell Signaling Technology (Beverly, MA, USA). Total cell lysate was precleared using protein L-Sepharose (Pierce Biotechnology, Rockford, IL, USA) or protein G-Sepharose (Sigma-Aldrich, St. Louis, MO, USA) at 4°C with 1 h of agitation. For each immunoprecipitation reaction, 400 microliters of the cleared lysate was incubated with 50 microliters MEM59 at 4°C overnight, and then 50 microliters protein L-Sepharose or protein G-Sepharose was added and incubated for an additional 1 h. Immunocomplexes were precipitated by centrifugation, washed three times with a radioimmunoprecipitation assay buffer [25 mmol/L Tris-HCl (pH 8.0), 150 mmol/L NaCl, 1% Nonidet P-40, a protease inhibitor mixture (Complete Mini EDTA-free, Roche Diagnostics, Mannheim, Germany)], and finally, resuspended in the sample buffer and boiled for 5 min. The released proteins were examined by Western blotting. Antibody against mouse Ig polycolonal antibody was used for control of the blot of the immunoprecipitate (Dako, Gostrup, Denmark). The intensity of the blot was measured by using LumiVision (Aishin, Nagoya, Japan).

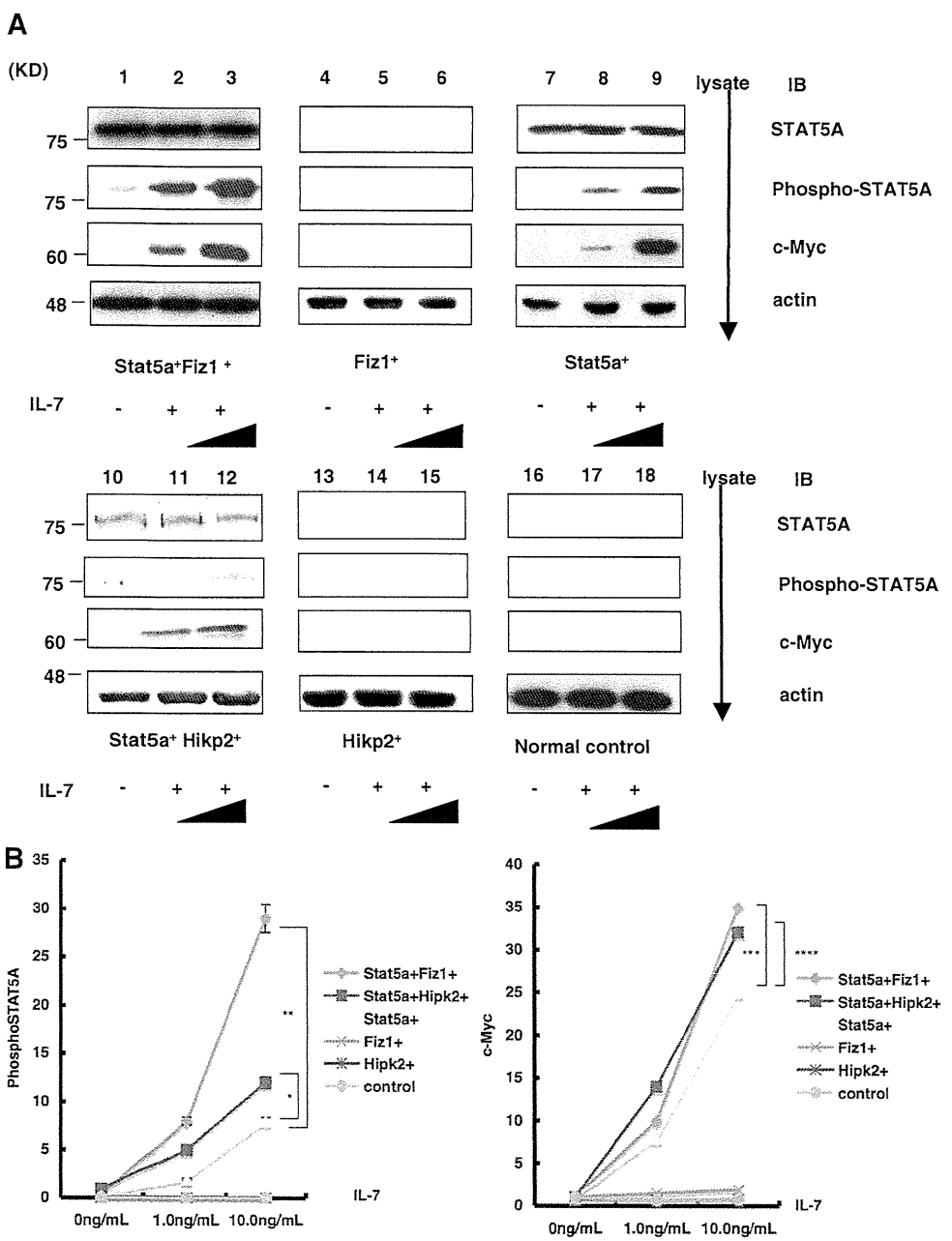

Figure 2. IL-7 induced phosphorylation of STAT5A and expression of c-Myc. (A) A representative blot of LBL cells with dual integration. Lanes 1, 4, 7, 10, 13, and 16, No IL-7 in the medium; lanes 2, 5, 8, 11, 14, and 17, 1.0 ng/mL IL-7; lanes 3, 6, 9, 12, 15, and 18, 10 ng/mL IL-7. IB, Immunoblot; Phospho, phosphorylated. (B) Intensity of phosphorylated STAT5A and c-Myc. The measurement was performed independently three times following IL-7R stimulation of the clone (the mean±SD; n=5).

RT-PCR

Total RNA was extracted from tissues using the ISOGEN reagent (Nippon Gene, Toyama, Japan). First-strand cDNA synthesis was performed using a Ready-To-Go T-primed first-strand kit (Amersham, Piscataway, NJ, USA). RT-PCR was performed as described previously [5]. The primers for β-actin were also prepared as reported previously. The primers for other genes were as follows: Igκ, 5′-GGCTGCAGSTCCAGTGGCAGTGGRTCWGGRA-3′ and 5′-CATTCCTGTTGAAGCTCTTGACAATGGGTG-3′; Igλ, 5′-GCCTTTCTACACTGCAGTGGGTATGCAACAAT-3′ and 5′-AGCCACTYACCTAGGACAGTSASYTTGGTTCC-3′ [25, 26]. A control β-actin probe was amplified by using RT-PCRmer™ β-actin (Gene Link, Hawthorne, NY, USA). For real-time RT-PCR, total RNA was reverse-transcribed using the Omniscript RT kit (Qiagen, Valencia, CA, USA). For relative quantification with RT-PCR, 20 ng each cDNA was analyzed using a FastStart DNA Master SYBR Green kit (Roche Diagnostics) with software, Version 3.5. For each primer pair, a standard curve was developed.

Statistical analysis

Analysis was done with the unpaired *t*-test. A P value <0.05 was considered to be statistically significant.

RESULTS

Identification of *Emv11* that is crucial for lymphomagenesis in SL/Kh mouse genome

In the current study, we found that studied SL/Kh mice share the *Emv11* that is mapped to 15.14cM on chromosome 7. Provirus *Emv11* was identified previously in strain AKR/J [27]. To study the susceptibility to pro-B cell lymphomagenesis by this proviral integration, we observed (SL/Kh×NFS/N)F1, backcrossed them to NFS/N, which did not possess pathogenic

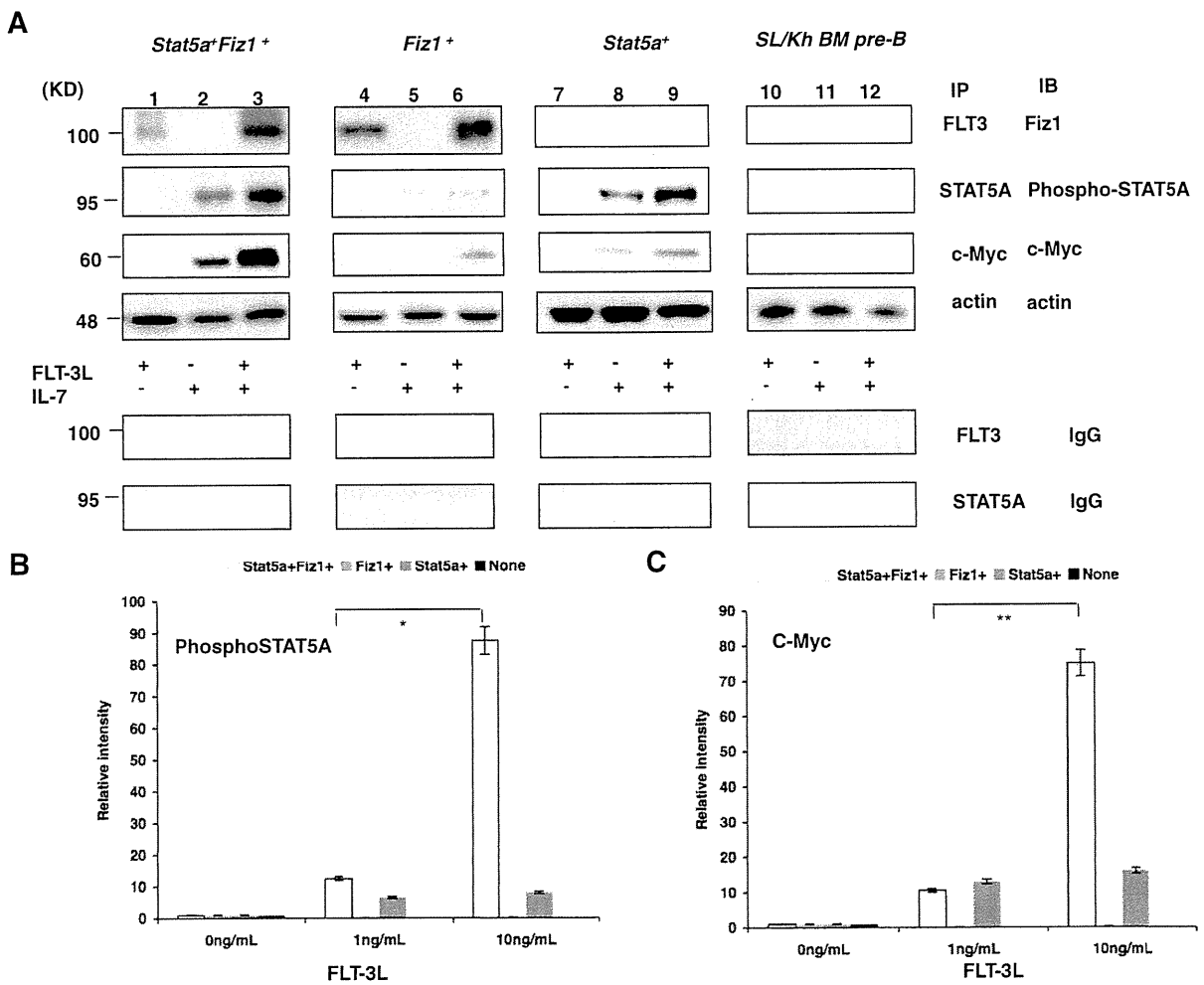

Figure 3. FLT3L induces phosphorylation of STAT5A and expression of c-Myc. (A) Blots of lymphoma cells with dual integration (*Stat5a*$^+$*Fiz1*$^+$) and single integration (*Stat5a*$^+$). Lanes 1, 4, 7, and 10, 1.0 ng/mL FLT3L and no IL-7; lanes 2, 5, 8, and 11, no FLT3L and 10 ng/mL IL-7; lanes 3, 6, 9, and 12, 1.0 ng/mL FLT3L and 10 ng/mL IL-7. IP, Immunoprecipitation. Normal control (no MLV integration) was BP-1$^+$B-220$^+$ BM pro-B cells from SL/Kh. (B) Relative intensity of phospho-STAT5A in immunoprecipitates in using an antibody recognizing STAT5A (the mean±SD; n=5). (C) Relative intensity of c-Myc in immunoprecipitates in using an antibody recognizing c-Myc (the mean±SD; n=5).

MLV, and analyzed spontaneous tumors. In F1, 32 of 62 (51%) individual mice developed pro-B cell lymphomas. In the backcross of the F1 to NFS/N, 38 of 102 (37.2%) mice developed lymphomas. Significantly, none of the backcross mice without the *Emv11* developed them. This evident cosegregation of lymphoma development with the *Emv11* plays a pivotal role in lymphomagenesis.

B-LBL clones with dual MLV integration

From primary B-LBL lymphomas of SL/Kh mice, we isolated several B-LBL clones with the *Emv11* integration(s) (**Table 1**). Southern blot analysis of *Nco*I- or *Sca*I-digested DNA with probes hybridizing to *Stat5a*, *Fiz1*, or *Hipk2* (**Fig. 1A**) revealed clonal rearrangements of these genes induced by the *Emv11* integration. FACScan analysis revealed that these clones were composed homogenously of BP-1$^+$ CD43$^+$ sIgM-B220$^+$ cells, indicating that the lymphoma cells were pro- to early pre-B cells (Fig. 1B). Histology of the lymphomas showed positive for Vpreb, one of the surrogate light chain components, and lymphoblastic morphology (Fig. 1C). PCR-Southern blot analysis of IgH rearrangement demonstrated monoclonal DQ52-J_H1 or -J_H2 rearrangement, indicating that the lymphoma cells used in this study were monoclonal (Fig. 1D, lanes 2–6). In addition, neither Igκ nor Igλ was detected in the lymphomas by the RT-PCR assay (Fig. 1E). The lymphoma clones used in this study are listed in Table 1.

Stimulation with IL-7R of B-LBL clones with double integration

Using these B-LBL clones, we studied the effect of IL-7R stimulation on STAT5A phosphorylation and induction of c-Myc, one of the downstream targets of STAT5A. Sorted BM pro-B cells were used as the control. It was found that the *Stat5a* target genes were commonly up-regulated in concomitance with the *Emv11* integration (**Fig. 2A**). After incubation in IL-7-free medium for 6 h, the B-LBL cells were added with 1.0 or 10.0 ng/ml IL-7 for 1 h. In B-LBL cells, with clonal *Stat5a* integration, the phosphorylation of STAT5A and the expression of c-Myc increased in a dose-dependent manner (Fig. 2A, lanes 2, 3, 8, 9, 11, and 12). In the absence of IL-7, phosphorylation of STAT5A and expression of c-Myc were nearly undetectable. Therefore, IL-7R stimulation was followed by STAT5a phosphorylation in B-LBL cells, with constitutive expression of STAT5A driven by the *Emv11* integration. Individual visualized blots of phosphorylated STAT5A and c-Myc were measured quantitatively (Fig. 2B). The results revealed that increases in STAT5A phosphorylation and c-Myc expression in the clones with the integration into the *Stat5a* and *Fiz1* or *Hipk2* were more than in the clones with the single integration into the *Stat5a* (*, P=0.003; **, P=0.004; ***, P=0.003; ****, P=0.012; Fig. 2B).

STAT5A phosphorylation was induced by stimulation of FLT3 with FLT3L in *Fiz1*$^+$ *Stat5a*$^+$ B-LBL cells

Next, we examined the effect of FLT3 stimulation with FLT3L on STAT5A phosphorylation. After 6 h in IL-7-free culture medium, B-LBL cells with the *Stat5a* and *Fiz1* integrations (*Stat5a*$^+$*Fiz1*$^+$) or with only *Stat5a* integration (*Stat5a*$^+$) were stimulated with 1.0 ng/mL FLT3L (**Fig. 3A**). IL-7 (1.0 ng/mL) was supplied again or not. The result revealed that in the *Stat5a*$^+$*Fiz1* and *Fiz1*$^+$ B-LBL cells, *Fiz1* was found to be associated with FLT3 when stimulated by FLT3L (Fig. 3A, lanes 1, 3, 4, and 6), and more phosphorylated STAT5A was observed following the supply of FLT3L (Fig. 3A, lanes 2 vs. 3 and 8 vs. 9). Moreover, we changed concentration of FLT3L from 1.0 ng/mL to 10 ng/mL and investigated the effects on phosphorylation of the STAT5A and c-Myc expression in the presence of 10 ng/mL IL-7. The result revealed that phosphorylation of STAT5A was increased in the *Stat5a*$^+$*Fiz1*$^+$ B-LBL cells following stimulation with 10 ng/mL FLT3L (Fig. 3B, lanes 2 vs. 3; *, P=0.008) but not in the *Stat5a*$^+$ clone (Fig. 3B, P=0.07). c-Myc expression was also up-regulated in the *Stat5a*$^+$*Fiz1*$^+$ clone following stimulation with 10 ng/mL FLT3L (Fig. 3B, *, P=0.012), but this up-regulation was not seen in the *Stat5a*$^+$ clone (Fig. 3B, P=0.051).

Colony growth of B-LBL cells on a semisolid medium

Next, we examined the effect of increased expression of these genes in the *Emv11* integration sites by culturing the cells on Methocult medium, semisolid methylcellulose medium containing 1.0 ng/mL IL-7, which was optimized for the culture of pre-B cells. We added 10 ng/mL FLT3L to the medium and observed the growth of *Stat5a*$^+$*Fiz1*$^+$ and *Stat5a*$^+$ clones, which began to grow after 48 h, forming col-

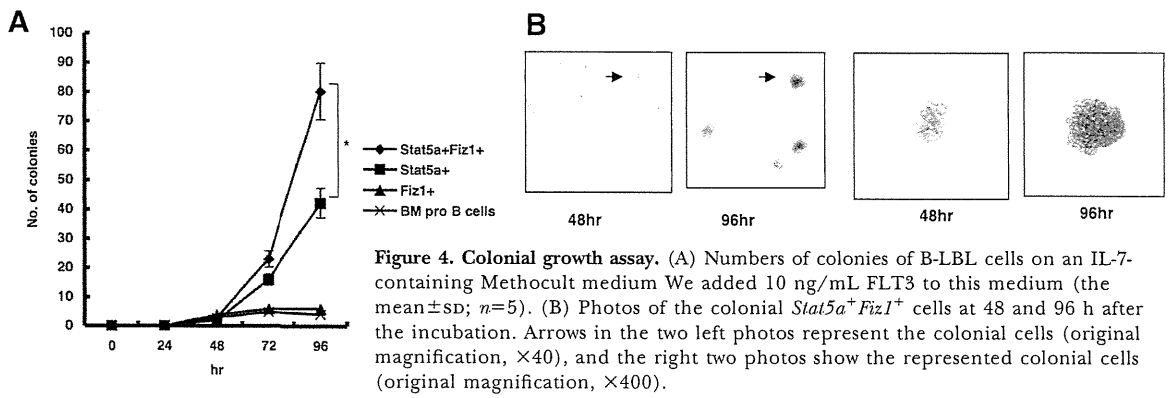

Figure 4. Colonial growth assay. (A) Numbers of colonies of B-LBL cells on an IL-7-containing Methocult medium We added 10 ng/mL FLT3 to this medium (the mean±SD; n=5). (B) Photos of the colonial *Stat5a*$^+$*Fiz1*$^+$ cells at 48 and 96 h after the incubation. Arrows in the two left photos represent the colonial cells (original magnification, ×40), and the right two photos show the represented colonial cells (original magnification, ×400).

onies in the semisolid medium. Colonies were grown on an average of six dishes that each contained 1.3×10^6 cells. Following the initial incubation, *Stat5a*$^+$*Fiz1*$^+$ clones grew faster than *Stat5a*$^+$ clones (**Fig. 4, A** and **B**). This result indicates that *Fiz1* up-regulation in expression promotes the growth of B-LBL cells with a supplement of FLT3L and IL-7 (*, P=0.003; Fig. 4A).

STAT5A phosphorylation was induced by stimulation with anti-CD43 in *Stat5a*$^+$*Hipk2*$^+$ B-LBL cells

Next, we examined the effect of CD43 stimulation by cross-linking in B-LBLs. After 6 h in IL-7-free medium, CD43 was cross-linked using an anti-CD43 antibody. The result revealed that *Hipk2* was found to be associated with CD43 following the cross-linking (**Fig. 5A**, lanes 1, 2, 7, and 8) in the *Stat5a*$^+$*Hipk2*$^+$ and *Hipk2*$^+$ clones. In the *Stat5a*$^+$*Hipk2*$^+$ clone, phosphorylated STAT5A was increased significantly by CD43 cross-linking in the *Stat5a*$^+$*Hipk2*$^+$ B-LBL cells (Fig. 5A, lanes 2 vs. 3; *, P=0.008; Fig. 5B) but not significantly in the *Stat5a* single integration clone (Fig. 5A, lanes 5 vs. 6; P=0.07; Fig. 5B). In close correlation with this, the significant increase in c-Myc expression in the *Stat5a*$^+$*Hipk2*$^+$ clones was observed following the cross-link (Fig. 5A; lanes 2 vs. 3; **, P=0.006; Fig. 5C), but it was not observed in the *Stat5a*$^+$ clones (Fig. 5A, lanes 5 vs. 6; P=0.09; Fig. 5C).

DISCUSSION

Constitutive activation of *Stat5a* by retrovirus integration contributes to lymphomagenesis via activation of the IL-7R signaling pathway [9]. In this study, we identified *Fiz1* and *Hipk2* as novel targets for integration. FLT3 is one of the markers and

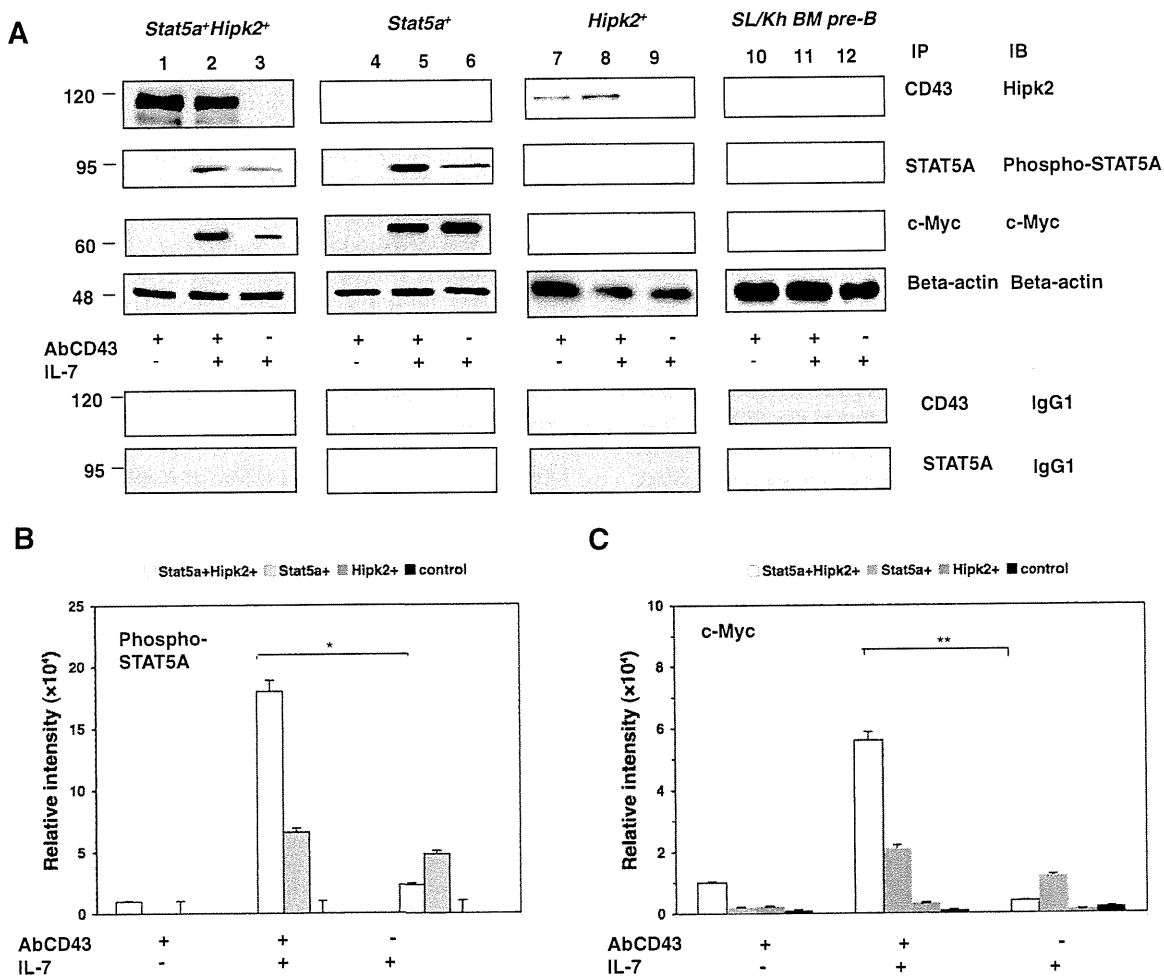

Figure 5. Cross-linking of CD43 induces phosphorylation of STAT5A and expression of c-Myc. (A) Lanes 1, 4, 7, and 10, No IL-7 with cross-linking; lanes 2, 5, 8, and 11, 1.0 ng/mL IL-7 with cross-linking; lanes 3, 6, 9, and 12, 1.0 ng/mL IL-7 without cross-linking. Anti-CD43 (AbCD43) was used at 20 ng/mL (lanes 1, 2, 4, 5, 7, 8, 10, and 11). (B) Relative intensity of phospho-STAT5A in blots of immunoprecipitates using an antibody recognizing phosphorylated STAT5A (the mean±SD; n=5). (C) Relative intensity of c-Myc in immunoblots of immunoprecipitates using an antibody recognizing c-Myc (the mean±SD; n=5).

functional molecules expressed in early B lymphoid progenitor cells [28–32]. As these pathways act selectively in the pro-B cell stage of B cell development, constitutive activation of these molecules may stabilize the immature host cellular phenotype and prevent further differentiation. Choudhary et al. [30] reported that STAT5A is involved in the FLT3 pathway. Mutations in the receptor tyrosine kinase FLT3 are a commonly occurring genetic lesion in acute myeloid leukemia [31]. ITD mutations clustered in the juxta-membrane domain are the most frequent and best-characterized type of mutation found in FLT3. FLT3-ITD-induced STAT5 activation is independent of Src, JAKs, and FLT3. The juxta-membrane domain of FLT3 is critical for ligand-dependent activation of FLT3 and for the transforming potential of oncogenic FLT3 mutants. In addition, phosphorylated STAT5 in the nucleus was detectable in 20% of B-lymphoblastic leukemia cells in the reported cases, and FLT3 is involved in B-acute lymphocytic leukemia with karyotype t (13; 13)(q12; q22) [32]. Thus, the FLT3 pathway can contribute to lymphomagenesis via STAT5A activation. We showed that the activation of the FLT3 pathway by increasing *Fiz1* expression may also contribute to STAT5 activation and B-LBL pathogenesis. As aforementioned, this pathway is enhanced by the supply of IL-7, suggesting the interaction between the IL-7R pathway and the FLT3 pathway.

In addition, we demonstrated a possibility that the CD43 pathway involved Hipk2 and STAT5A. In T cell development, TCR-dependent cell response is modulated by CD43 engagement [33]. Lee et al. [34] demonstrated that *Hipk2* promotes Wnt/Wg signaling by stabilizing β-catenin/Armadillo and stimulating target gene expression. This group also showed that *Hipk2* interacts with lymphoid-enhancing factor 1, which acts as a transcriptional factor, promoting c-Myc and cyclin D1 expression. In the erythroleukemic cell line TF-1, STAT5A is not associated with CD43-mediated cell proliferation [35]. Recently, it was found that CD43 functions as an E-selectin counter-receptor in human pre-B cell leukemia NALL-1 cell line [36]. Thus, CD43 signaling pathway is one of the candidate pathways that actively operates in the B-LBLs. In our study, CD43 cross-linking resulted in an increase in STAT5A phosphorylation and c-Myc expression in *Stat5a*$^{+}$*Hipk2*$^{+}$ B-LBL cells when IL-7 was supplied. These data suggest that CD43 enhances the IL-7R signal pathway, which normally enhances c-Myc expression via STAT5A phosphorylation. Taken together, we propose a scheme of interactions among the IL-7, CD43, and FLT3 signaling pathways (**Fig. 6**). Thus, we hypothesize that these three pathways form an interacting network and affect B-LBL development. SL/Kh mice serve as one of the appropriate models for studying the signaling pathways leading to lymphomagenesis, using MLV integration as a tool. The data we report here will provide new insights into the aberrant signaling pathways leading to lymphomagenesis.

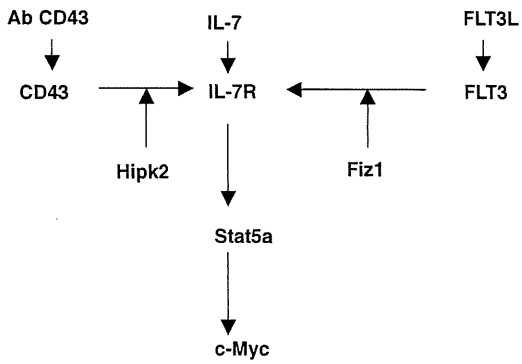

Figure 6. Plausible signaling pathways in B-LBL cells.

AUTHORSHIP

Tatsuaki Tsuruyama planned all of the experiments. Tatsuaki Tsuruyama, Yukiko Imai, Haruya Takeuchi, Takuya Hiratsuka, Yasuhiro Maruyama, Kazuya Kanaya, Richard Kaszynski, and Guang Jin conducted all of the experiments. Tatsuaki Tsuruyama, Tomoko Okuno, Munetaka Ozeki, Takuro Nakamura, Tetsuya Takakuwa, Toshiaki Manabe, and Hiroshi Hiai critically advised on the signaling pathway and morphology of the lymphoma tissue. Tatsuaki Tsuruyama and Keiji Tamaki analyzed the data. Tatsuaki Tsuruyama and Richard Kaszynski wrote the paper.

ACKNOWLEDGMENTS

This work was supported by a grant-in-aid for cancer research from the Ministry of Education, Culture, Sports, Science, and Technology, Japan, and a grant for strategic research on cancer from the Ministry of Health, Labor, and Welfare, Japan. We are grateful for the generous financial support from the Kyoto Shimizu Immunology Foundation.

REFERENCES

1. Coffin, J. M., Hughes, S. H., Varmus, H. E. (1997) *Retroviruses.* New York, NY, USA, Cold Spring Harbor Laboratory.
2. Suzuki, T., Shen, H., Akagi, K., Morse, H. C., Malley, J. D., Naiman, D. Q., Jenkins, N. A., Copeland, N. G. (2002) New genes involved in cancer identified by retroviral tagging. *Nat. Genet.* **32,** 166–174.
3. Abujiang, P., Yamada, Y., Haller, O., Kobayashi, H., Kamoto, T., Lu, L. M., Ogawa, M., Ishimoto, A., Katoh, H., Kanehira, K., Ikegami, S., Fukumoto, M., Hiai, H. (1996) The origin of SL family mice. *Lab. Anim. Sci.* **46,** 410–417.
4. Hiai, H., Yamada, Y., Abujiang, P., Lu, L., Kamoto, T., Tsuruyama, T. (1999) Genetic and epigenetic susceptibility to endogenous retrovirus-induced lymphomas in SL mice. *Prog. Exp. Tumor Res.* **35,** 64–77.
5. Shimada, M. O., Yamada, Y., Nakakuki, Y., Okamoto, K., Fukumoto, M., Honjo, T., Hiai, H. (1993) SL/KH strain of mice: a model of spontaneous pre-B-lymphomas. *Leuk. Res.* **17,** 573–578.
6. Lu, L-M., Shimada, M., Higashi, S., Zeng, Z-Z., Hiai, H. (1999) Bone marrow pre-B-1 (Bomb1): a quantitative trait locus inducing bone marrow pre-B cell expansion in lymphoma-prone SL/Kh mice. *Cancer Res.* **59,** 2593–2595.
7. Moll, B., Hartley, J. W., Rowe, W. P. (1979) Induction of B-tropic and N-tropic murine leukemia virus from B10.BR/SgLi mouse embryo cell lines by 5-iodo-2′-deoxyuridine. *J. Natl. Cancer Inst.* **63,** 213–217.
8. Hiratsuka, T., Tsuruyama, T., Kaszynski, R., Kometani, K., Minato, N., Nakamura, T., Tamaki, K., Hiai, H. (2008) Bone marrow pre-B expansion by SL/Kh-Bomb1 locus: not sufficient for lymphomagenesis. *Leuk. Res.* **32,** 309–314.
9. Tsuruyama, T., Nakamura, T., Jin, G., Ozeki, M., Yamada, Y., Hiai, H. (2002) Constitutive activation of *Stat5a* by retrovirus integration in early pre-B lymphomas of SL/Kh strain mice. *Proc. Natl. Acad. Sci. USA* **99,** 8253–8258.
10. Jin, G., Tsuruyama, T., Yamada, Y., Hiai, H. (2003) Svi3: a provirus common integration site in c-myc in SL/Kh pre-B lymphomas. *Cancer Sci.* **94,** 791–795.

11. Wu, X., Li, Y., Crise, B., Burgess, S. M. (2003) Transcription start regions in the human genome are favored targets for MLV integration. *Science* **300,** 1749–1751.
12. Ihle, J. N. (2001) The Stat family in cytokine signaling. *Curr. Opin. Cell Biol.* **13,** 211–217.
13. Matsumura, I., Kitamura, T., Wakao, H., Tanaka, H., Hashimoto, K., Albanese, C., Downward, J., Pestell, R. G., Kanakura, Y. (1999) Transcriptional regulation of the cyclin D1 promoter by STAT5: its involvement in cytokine-dependent growth of hematopoietic cells. *EMBO J.* **18,** 1367–1377.
14. Nosaka, T., Kawashima, T., Misawa, K., Ikuta, K., Mui, A. L., Kitamura, T. (1999) STAT5 as a molecular regulator of proliferation, differentiation, and apoptosis in hematopoietic cells. *EMBO J.* **18,** 4754–4765.
15. Lanvin, O., Gouilleux, F., Mullié, C., Mazière, C., Fuentes, V., Bissac, E., Dantin, F., Mazière, J. C., Régnier, A., Lassoued, K., Gouilleux-Gruart, V. (2004) Interleukin-7 induces apoptosis of 697 pre-B cells expressing dominant-negative forms of STAT5: evidence for caspase-dependent and -independent mechanisms. *Oncogene* **23,** 3040–3047.
16. Sexl, V., Piekorz, R., Moriggl, R., Rohrer, J., Brown, M. P., Bunting, K. D., Rothammer, K., Roussel, M. F., Ihle, J. N. (2000) *Stat5a/b* contribute to interleukin 7-induced B-cell precursor expansion, but abl- and bcr/abl-induced transformation are independent of stat5. *Blood* **96,** 2277–2283.
17. Dai, X., Chen, Y., Di, L., Podd, A., Li, G., Bunting, K. D., Hennighausen, L., Wen, R., Wang, D. (2007) Stat5 is essential for early B cell development but not for B cell maturation and function. *J. Immunol.* **179,** 1068–1079.
18. Sudo, T., Ito, M., Ogawa, Y., Iizuka, M., Kodama, H., Kunisada, T., Hayashi, S., Ogawa, M., Sakai, K., Nishikawa, S. (1989) Interleukin 7 production and function in stromal cell-dependent B cell development. *J. Exp. Med.* **170,** 333–338.
19. Funk, P. E., Stephan, R. P., Witte, P. L. (1995) Vascular cell adhesion molecule 1-positive reticular cells express interleukin-7 and stem cell factor in the bone marrow. *Blood* **86,** 2661–2671.
20. Malin, S., McManus, S., Cobaleda, C., Novatchkova, M., Delogu, A., Bouillet, P., Strasser, A., Busslinger, M. (2010) Role of STAT5 in controlling cell survival and immunoglobulin gene recombination during pro-B cell development. *Nat. Immunol.* **11,** 171–179.
21. Hardy, R. R., Carmack, C. E., Shinton, S. A., Kemp, J. D., Hasegawa, K. (1991) Resolution and characterization of pro-B and pre-pro-B cells stage in normal mouse bone marrow. *J. Exp. Med.* **173,** 1213–1225.
22. Wolf, I., Rohrschneider, L. R. (1999) *Fiz1,* a novel zinc finger protein interacting with the receptor tyrosine kinase Flt3. *J. Biol. Chem.* **274,** 21478–21484.
23. Wang, W., Link, V., Green, J. M. (2000) Identification and cloning of a CD43-associated serine/threonine kinase. *Cell. Immunol.* **205,** 34–39.
24. Sakano, H., Maki, R., Kurosawa, Y., Roeder, W., Tonegawa, S. (1980) Two types of somatic recombination are necessary for the generation of complete immunoglobulin heavy-chain genes. *Nature* **286,** 676–683.
25. Sakano, H., Huppi, K., Heinrich, G., Tonegawa, S. (1979) Sequences at the somatic recombination sites of immunoglobulin light-chain genes. *Nature* **280,** 288–294.
26. Da Sylva, T. R., Fong, I. C., Cunningham, L. A., Wu, G. E. (2007) RAG1/2 re-expression causes receptor revision in a model B cell line. *Mol. Immunol.* **44,** 889–899.
27. Lenz, J., Crowther, R., Straceski, A., Haseltine, W. (1982) Nucleotide sequence of the Akv env gene. *J. Virol.* **42,** 519–529.
28. Rappold, I., Ziegler, B. L., Köhler, I., Marchetto, S., Rosnet, O., Birnbaum, D., Simmons, P. J., Zannettino, A. C., Hill, B., Neu, S., Knapp, W., Alitalo, R., Alitalo, K., Ullrich, A., Kanz, L., Bühring, H. J. (1997) Functional and phenotypic characterization of cord blood and bone marrow subsets expressing FLT3 (CD135) receptor tyrosine kinase. *Blood* **90,** 111–125.
29. Ogawa, M., Sugawara, S., Kunisada, T., Sudo, T., Hayashi, S., Nishikawa, S., Kodama, H., Nishikawa, S. (1998) Flt3/Flk-2 and c-Kit are not essential for the proliferation of B lymphoid progenitor cells in the bone marrow of the adult mouse. *Exp. Hematol.* **26,** 478–488.
30. Choudhary, C., Brandts, C., Schwable, J., Tickenbrock, L., Sargin, B., Ueker, A., Böhmer, F. D., Berdel, W. E., Müller-Tidow, C., Serve, H. (2007) Activation mechanisms of STAT5 by oncogenic Flt3-ITD. *Blood* **110,** 370–374.
31. Vempati, S., Reindl, C., Wolf, U., Kern, R., Petropoulos, K., Naidu, V. M., Buske, C., Hiddemann, W., Kohl, T. M., Spiekermann, K. (2008) Transformation by oncogenic mutants and ligand-dependent activation of FLT3 wild-type requires the tyrosine residues 589 and 591. *Clin. Cancer Res.* **14,** 4437–4445.
32. Tzankov, A., Sotlar, K., Muhlematter, D., Theocharides, A., Went, P., Jotterand, M., Horny, H. P., Dirnhofer, S. (2008) Systemic mastocytosis with associated myeloproliferative disease and precursor B lymphoblastic leukemia with t(13)13)(q12)q22) involving FLT3. *J. Clin. Pathol.* **61,** 958–961.
33. Fierro, N. A., Pedraza-Alva, G., Rosenstein, Y. (2006) TCR-dependent cell response is modulated by the timing of CD43 engagement. *J. Immunol.* **176,** 7346–7353.
34. Lee, W., Swarup, S., Chen, J., Ishitani, T., Verheyen, E. M. (2009) Homeodomain-interacting protein kinases (Hipks) promote Wnt/Wg signaling through stabilization of β-catenin/Arm and stimulation of target gene expression. *Development* **136,** 241–251.
35. Miura, Y., Mizutani, C., Nishihara, T., Hishita, T., Yanagi, S., Tohyama, Y., Ichiyama, S., Yamamura, H., Uchiyama, T., Tohyama, K. (2001) Adhesion via CD43 induces Syk activation and cell proliferation in TF-1 cells. *Biochem. Biophys. Res. Commun.* **288,** 80–86.
36. Nonomura, C., Kikuchi, J., Kiyokawa, N., Ozaki, H., Mitsunaga, K., Ando, H., Kanamori, A., Kannagi, R., Fujimoto, J., Muroi, K., Furukawa, Y., Nakamura, M. (2008) CD43, but not P-selectin glycoprotein ligand-1, functions as an E-selectin counter-receptor in human pre-B-cell leukemia NALL-1. *Cancer Res.* **68,** 790–799.

KEY WORDS:
murine leukemia · Stat5a · B-LBL · Flt3 · CD43

Journal of General Virology (2010), **91**, 773–781 DOI 10.1099/vir.0.017368-0

Small intestine $CD4^+$ cell reduction and enteropathy in simian/human immunodeficiency virus KS661-infected rhesus macaques in the presence of low viral load

Katsuhisa Inaba,[1] Yoshinori Fukazawa,[1] Kenta Matsuda,[1] Ai Himeno,[1] Megumi Matsuyama,[1] Kentaro Ibuki,[1] Yoshiharu Miura,[2] Yoshio Koyanagi,[2] Atsushi Nakajima,[3] Richard S. Blumberg,[4] Hidemi Takahashi,[5] Masanori Hayami,[1] Tatsuhiko Igarashi[1] and Tomoyuki Miura[1]

Correspondence
Tomoyuki Miura
tmiura@virus.kyoto-u.ac.jp

[1]Laboratory of Primate Model, Experimental Research Center for Infectious Diseases, Institute for Virus Research, Kyoto University, 53 Shogoinkawaramachi, Sakyo-ku, Kyoto 606-8507, Japan

[2]Laboratory of Viral Pathogenesis, Institute for Virus Research, Kyoto University, 53 Shogoinkawaramachi, Sakyo-ku, Kyoto 606-8507, Japan

[3]Division of Gastroenterology, Yokohama City University Graduate School of Medicine, Yokohama, Japan

[4]Division of Gastroenterology, Brigham and Women's Hospital, Harvard Medical School, Boston, MA, USA

[5]Department of Microbiology and Immunology, Nippon Medical School, Tokyo, Japan

Human immunodeficiency virus type 1, simian immunodeficiency virus and simian/human immunodeficiency virus (SHIV) infection generally lead to death of the host accompanied by high viraemia and profound $CD4^+$ T-cell depletion. SHIV clone KS661-infected rhesus macaques with a high viral load set point (HVL) ultimately experience diarrhoea and wasting at 6–12 months after infection. In contrast, infected macaques with a low viral load set point (LVL) usually live asymptomatically throughout the observation period, and are therefore referred to as asymptomatic LVL (Asym LVL) macaques. Interestingly, some LVL macaques exhibit diarrhoea and wasting similar to the symptoms of HVL macaques and are termed symptomatic LVL (Sym LVL) macaques. This study tested the hypothesis that Sym LVL macaques have the same degree of intestinal abnormalities as HVL macaques. The proviral DNA loads in lymphoid tissue and the intestines of Sym LVL and Asym LVL macaques were comparable and all infected monkeys showed villous atrophy. Notably, the $CD4^+$ cell frequencies of lymphoid tissues and intestines in Sym LVL macaques were remarkably lower than those in Asym LVL and uninfected macaques. Furthermore, Sym LVL and HVL macaques exhibited an increased number of activated macrophages. In conclusion, intestinal disorders including $CD4^+$ cell reduction and abnormal immune activation can be observed in SHIV-KS661-infected macaques independent of virus replication levels.

Received 5 October 2009
Accepted 3 November 2009

INTRODUCTION

The intestinal tract, which is the largest mucosal and lymphoid organ and which contains the majority of the total lymphocytes in the body, is an important port of entry for human immunodeficiency virus type 1 (HIV-1) infection in vertical and homosexual transmission (Smith *et al.*, 2003). Additionally, the intestinal tract is a central site in the interaction between HIV-1 and its host, and suffers profound pathological changes as a result of HIV-1 infection. HIV-1 infection of the intestinal tract is characterized by virus replication (Fackler *et al.*, 1998), $CD4^+$ T-cell depletion (Brenchley *et al.*, 2004), opportunistic infection and HIV enteropathy, which is an idiopathic intestinal disorder observed in infected patients with diarrhoea (Kotler, 2005). In particular, $CD4^+$ T-cell depletion, which is the immunological hallmark in the development of AIDS, preferentially takes place in the intestinal tract rather than in the peripheral blood throughout the infection (Brenchley *et al.*, 2004). This

observation is based on the following findings: (i) most naturally transmitted HIV-1 strains are chemokine receptor 5 (CCR5)-tropic; and (ii) the intestinal tract, especially the lamina propria, contains a large number of activated memory $CCR5^+$ $CD4^+$ T cells, which indicates a high susceptibility for HIV-1 infection, whereas the peripheral blood has a relatively small population of these cells (Anton *et al.*, 2000; Lapenta *et al.*, 1999). $CD4^+$ T-cell depletion from the intestinal tract by HIV-1 infection is thought to lead to progressive dysfunction of mucosal immunity, which triggers immunodeficiency (Paiardini *et al.*, 2008). In addition to $CD4^+$ T-cell depletion in the intestinal tract, HIV-1 infection causes histopathological changes in the intestine, including villous atrophy, crypt hyperplasia and acute/chronic inflammation (Batman *et al.*, 1989).

Chronic disease of the intestinal tract generally manifests as inflammation (Kahn, 1997). Diarrhoea is a major intestinal symptom caused by various stimuli to the intestinal tract such as pathogens, toxins and dysfunction of the immune system (Gibbons & Fuchs, 2007). Because HIV-1 infection weakens the host immune system, AIDS is one of the primary causes of chronic diarrhoea (Sestak, 2005). In developing countries, diarrhoea was a major symptom in advanced HIV-1 infection prior to the establishment of highly active antiretroviral therapy (HAART) (Wilcox & Saag, 2008). Dehydration and malabsorption as a result of chronic diarrhoea can lead to progressive weight loss and can contribute to morbidity and mortality in HIV-1-infected patients (Sharpstone & Gazzard, 1996). Therefore, chronic diarrhoea is one of the most important clinical signs in AIDS patients.

AIDS models using non-human primates have provided many important observations on AIDS pathogenesis. The first finding of early $CD4^+$ T-cell depletion from the intestinal tract was reported in a study using simian immunodeficiency virus (SIV)-infected macaques (Veazey *et al.*, 1998). Intestinal $CD4^+$ T cells of rhesus macaques predominantly exhibit a $CCR5^+$ activated memory phenotype, and $CD4^+$ T cells of this phenotype are selectively eliminated in SIV-infected macaques, indicating that the majority of intestinal $CD4^+$ T cells are primary targets of SIV infection (Veazey *et al.*, 2000a, b). Accordingly, detailed analysis of the intestinal tract using animal models is essential for an understanding of AIDS pathogenesis.

Simian/human immunodeficiency virus (SHIV)-KS661 is a molecular clone and a pathogenic virus in rhesus macaques. SHIV-KS661 systemically depletes $CD4^+$ T cells of rhesus macaques within 4 weeks of infection (Miyake *et al.*, 2006). Based on our observations over a number of years, intravenous infection of rhesus macaques with SHIV-KS661 consistently results in high viraemia and $CD4^+$ T-cell depletion, followed by malignant morbidity as a result of severe chronic diarrhoea and wasting after 6–18 months. Generally, the time to clinical morbidity in rhesus macaques infected with pathogenic SHIVs, such as SHIV-89.6P and SHIV-KS661, is considerably shorter than in HIV-1-infected humans, who take an average of 10 years to progress to AIDS. In addition, all subsets of $CD4^+$ T cells including memory and naïve T cells are thoroughly depleted in pathogenic SHIV-infected macaques. However, in the SHIV-KS661 macaque model, diarrhoea and wasting, which are major symptoms in advanced HIV-1 infection, can clearly be recognized and defined in association with disease progression.

Recently, we observed that, in many rhesus macaques infected intrarectally with SHIV-KS661, plasma viral RNA loads decreased gradually to undetectable levels in the chronic phase, which is quite different from the case with intravenous infection. It is well known that pathogenic SIV and SHIV infections in monkeys, like HIV-1 infections in humans, generally lead to high viraemia, profound $CD4^+$ T-cell depletion and death. Interestingly, in this study, two out of six intrarectally inoculated macaques with a low plasma viral load experienced malignant morbidity manifest as severe diarrhoea and wasting, similar to what we observed in infected macaques with high viraemia. The purpose of this study was to elucidate why macaques with a low plasma viral load experienced diarrhoea and wasting. As an explanation for this morbidity, we hypothesized that, even if the viral load set-point is suppressed, SHIV-KS661-infected macaques would have the same degree of intestinal abnormalities as infected macaques with high viraemia. To test this hypothesis, we analysed $CD4^+$ cell frequencies in lymphoid and intestinal tissues and damage to the intestinal mucosa in infected macaques with high and low viral load set points (HVL and LVL, respectively). Here, we have provided evidence for the development of intestinal disorders in SHIV-KS661-infected macaques irrespective of the plasma viral RNA load.

RESULTS

Diarrhoea and wasting in two macaques despite low viral load

All macaques inoculated intravenously with SHIV-KS661 and one out of seven macaques inoculated intrarectally with SHIV-KS661 exhibited high set points of plasma viral RNA loads, persisting at over 10^6 copies ml^{-1} until they needed to be euthanized as a result of diarrhoea and wasting (Fig. 1a). In contrast, in the remaining six macaques inoculated intrarectally with SHIV-KS661, the set points of plasma viral RNA load gradually decreased to undetectable levels (Fig. 1a). We called these macaques showing high and low set points of viral RNA load HVL and LVL macaques, respectively. During an observation period of approximately 1.4 years, two LVL macaques (MM397 and MM399) experienced severe diarrhoea and wasting and required euthanasia at approximately 22 weeks post-infection (p.i.), similar to HVL macaques, whereas the remaining four LVL macaques were asymptomatic (Fig. 1a). We termed the healthy LVL macaques asymptomatic LVL macaques (Asym LVL) and the LVL

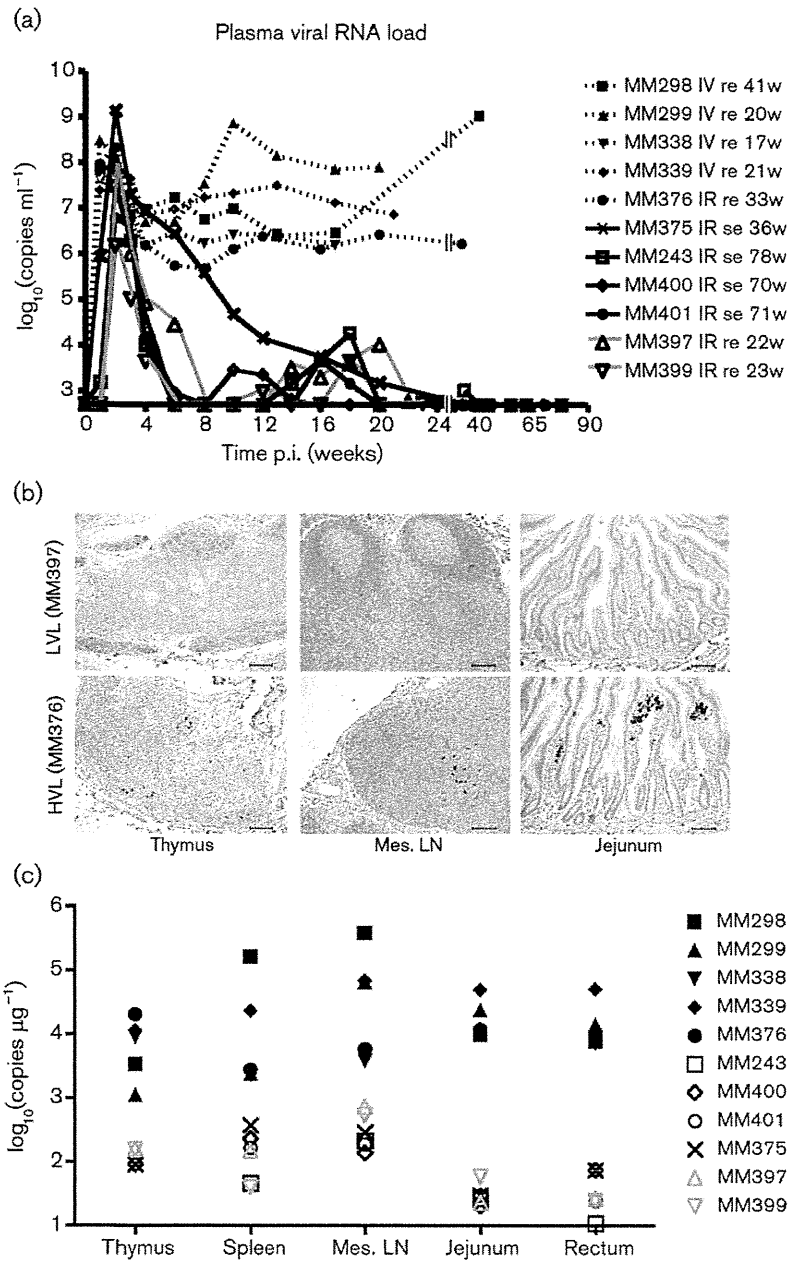

Fig. 1. Distribution of virus in various tissues of SHIV-KS661-infected rhesus macaques. (a) Time course of plasma viral RNA loads as measured by quantitative RT-PCR. The detection limit of plasma viral RNA loads was 500 copies ml^{-1}. The animal ID numbers, infection route and when and how they were euthanized are indicated on the figure. IV, Intravenous inoculation; IR, intrarectal inoculation; re, required euthanasia; se, scheduled euthanasia; w, number of weeks after infection when euthanasia was performed. (b) Immunohistochemical detection of Nef antigen in thymus, mesenteric lymph nodes (Mes. LN) and jejunum. Brown staining indicates Nef^+ cells. The upper panels show representative tissue sections from a Sym LVL macaque (MM397) and the lower panels show representative tissue sections from an HVL macaque (MM376). Bars, 100 µm. (c) Proviral DNA loads in different tissues of SHIV-KS661-infected macaques, as measured by quantitative PCR. The detection limit of proviral DNA loads was 10 copies μg^{-1}. Filled black symbols indicate HVL macaques, open black symbols indicate Asym LVL macaques and open grey symbols indicate Sym LVL macaques.

macaques with diarrhoea and wasting symptomatic LVL macaques (Sym LVL).

Antibody response against SHIV in infected macaques

The LVL macaques showed antibody responses to SHIV-KS661 at 3–4 weeks p.i. and then developed strong antibody responses that persisted up to 18 weeks p.i. (Table 1). In contrast, two of the HVL macaques (MM298 and MM299) showed no antibody response, whilst the remaining two (MM338 and MM339) showed very low antibody responses. Among the HVL macaques, only MM376 showed a strong antibody response: the titre reached 1 : 2048 at 6 weeks p.i., but then decreased to a much lower value. These results showed that LVL macaques succeeded in maintaining a strong antibody response, whilst HVL macaques failed to do so.

Viral levels in tissues from Sym LVL and Asym LVL macaques are not significantly different

To investigate whether the infected macaques had different viral levels in their lymphoid and intestinal tissues, we used

Table 1. Anti-HIV antibody titres in infected monkeys

– indicates a titre of <32.

Time (weeks)	Intrarectal inoculation						Intravenous inoculation				
	LVL						HVL				
	MM243	MM397	MM399	MM400	MM401	MM375	MM376	MM298	MM299	MM338	MM339
0	–	–	–	–	–	–	–	–	–	–	–
1	–	–	–	–	–	–	–	–	–	–	–
2	–	–	–	–	–	–	–	–	–	64	64
3	32	–	32	–	–	128	–	–	–	32	32
4	32	16384	32	64	32	512	512	–	–	–	–
6	8192	16384	256	64	4096	1024	2048	–	–	–	–
8	4096	16384	1024	128	1024	16384	512	–	–	–	–
10	16384	16384	2048	512	512	16384	512	–	–	–	–
12	16384	16384	256	512	4096	16384	512				
13								–	–	–	–
14	16384	16384	1024	512	2048						
16	4096	8192	1024	1024	1024	16384	64				
17								–	–	–	–
18	8192	16384	2048	8192	4096						

the Nef antigen as a marker of virus infection using immunohistochemistry and quantitative analysis of proviral DNA in lymphoid and intestinal tissues. Nef^+ cells were detected in large numbers in the tissues of HVL macaques, but were undetectable in both Sym LVL (Fig. 1b) and Asym LVL (data not shown) macaques.

In the HVL macaques, high proviral DNA loads (>1000 copies μg^{-1}) were found in all of the tissues examined (Fig. 1c). In contrast, the proviral DNA loads in the tissues of the LVL macaques were only several tens to several hundreds of copies μg^{-1} (Fig. 1c). Furthermore, Sym LVL and Asym LVL macaques exhibited comparably low proviral DNA loads in these tissues (Fig. 1c). The low viral levels in lymphoid and intestinal tissues in the LVL macaques were consistent with their set points of plasma viral RNA loads. The viral levels in lymphoid and intestinal tissues were not significantly different between Sym LVL and Asym LVL macaques.

Diarrhoea and wasting in LVL macaques correlate with $CD4^+$ cell frequency in lymphoid and intestinal tissues, but not in peripheral blood

Because $CD4^+$ T-cell depletion is the hallmark of AIDS, we first examined $CD4^+$ T-cell counts in peripheral blood. Whilst peripheral $CD4^+$ T cells were completely and irreversibly depleted in HVL macaques throughout the infection, they displayed various kinetics in LVL macaques (Fig. 2a). MM397 (Sym LVL) and MM401 (Asym LVL) had very low $CD4^+$ T-cell counts (<150 cells ml^{-1}) at all times at which they were examined after infection, whereas MM399 (Sym LVL) and MM400 (Asym LVL) maintained moderate $CD4^+$ T-cell counts (>300 cells ml^{-1}) throughout the experiment (Fig. 2a).

Naïve $CD4^+$ T cells of MM397 (Sym LVL), MM243 (Asm LVL) and MM401 (Asym LVL) were depleted as early as 4 weeks p.i., whereas those of MM399 (Sym LVL) and MM400 (Asym LVL) remained at moderate levels (Fig. 2b). The HVL macaques were not examined because their peripheral $CD4^+$ T cells were depleted.

In addition to evaluating $CD4^+$ T cells in the blood, we evaluated $CD4^+$ cells in lymphoid and intestinal tissues using CD4 staining. The HVL macaques showed severe depletion of $CD4^+$ cells in all lymphoid tissues and intestine compared with the uninfected macaques (Fig. 2c, d). Interestingly, the $CD4^+$ cell frequencies in the tissues were clearly lower in Sym LVL macaques than in uninfected macaques (Fig. 2c, d). However, the $CD4^+$ cell frequencies in the tissues of Asym LVL macaques were comparable to those in uninfected macaques. These findings indicated that the emergence of diarrhoea and wasting in LVL macaques correlated with the low $CD4^+$ cell frequency in lymphoid tissues and the intestines, but not with the counts of peripheral $CD4^+$ T-cell subsets.

Infected animals exhibit significantly shorter villi

Symptomatic animals (Sym LVL and HVL macaques) exhibited diarrhoea. To examine whether the jejunum of symptomatic animals exhibited the histopathological changes that suggest AIDS-related enteropathy, we measured villous length on haematoxylin and eosin (H&E)-stained samples of jejunum in uninfected and infected macaques. Surprisingly, villous length was significantly

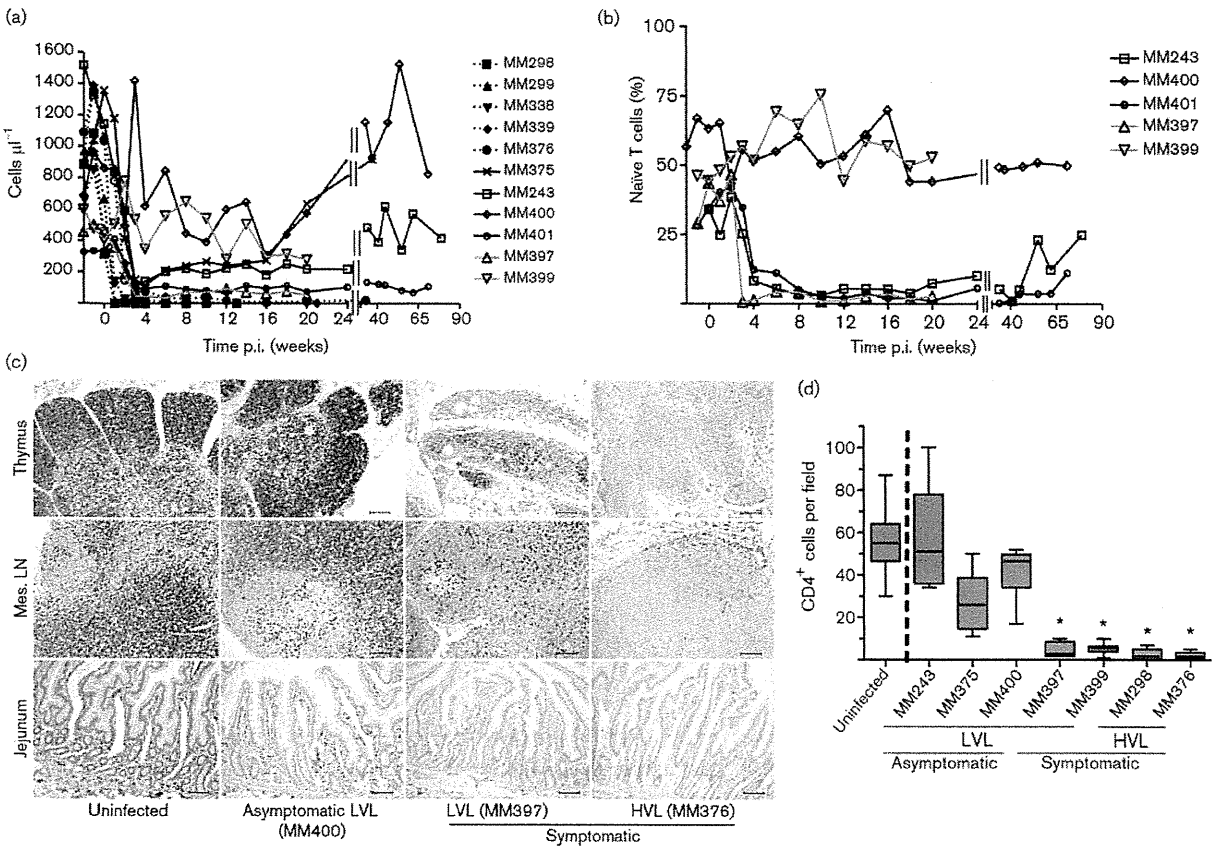

Fig. 2. Counts of circulating $CD4^+$ T-cell subsets and $CD4^+$ cell frequency in lymphoid and intestinal tissues at the time of euthanasia in SHIV-KS661-infected rhesus macaques. Counts of circulating $CD4^+$ T-cell subsets were analysed by flow cytometry and whole-blood counts. (a) Circulating $CD4^+$ T-cell counts. The ID numbers of the macaques are indicated on the figure. (b) Proportion of $CD95^+$ naïve cells in circulating $CD4^+$ T cells of LVL macaques. Solid black lines indicate Asym LVL macaques and solid grey lines indicate Sym LVL macaques. (c) $CD4^+$ cell frequencies in thymus, mesenteric lymph nodes (Mes. LN) and jejunum of representative uninfected, Asym LVL, Sym LVL and HVL macaques. Bars, 100 μm. (d) Quantification of jejunum $CD4^+$ cells in uninfected and infected macaques. The numbers of $CD4^+$ cells were enumerated in at least ten fields of the tissues at a magnification of 200×. Statistical analysis was performed using Student's *t*-test for the data from five uninfected and each infected macaque (*, $P<0.0001$). Data for MM299, MM338, MM339 and MM401 were not available.

shorter in all of the infected animals than in uninfected animals ($P<0.0001$) (Fig. 3a, b). This suggested that SHIV-infected animals develop villous atrophy, irrespective of viral load.

Increased number of activated macrophages in the jejunum of symptomatic animals

Macrophages appeared to be more abundant in H&E-stained jejunal sections in symptomatic animals. This was confirmed by CD68 staining: the frequency of $CD68^+$ macrophages in the jejunum was considerably higher in symptomatic animals than in uninfected animals, but was not significantly different between uninfected animals and Asym LVL macaques (data not shown). Furthermore, $CD68^+$ macrophages in the small intestine of Sym LVL and HVL macaques appeared to be activated because their size was increased. To examine whether the number of activated $CD68^+$ macrophages increased in the small intestine, we double stained for CD68 and Ki67 in the small intestine sections by immunohistochemistry. The frequency of $CD68^+$ $Ki67^+$ macrophages in the jejunum of all symptomatic animals examined was significantly higher than that of uninfected animals ($P<0.0001$) (Fig. 3c, d). This suggested that abnormal activation of intestinal macrophages occurred in symptomatic animals irrespective of viral load.

DISCUSSION

It is important to discuss initially why some SHIV-infected macaques had an HVL at the late stage, whilst others had

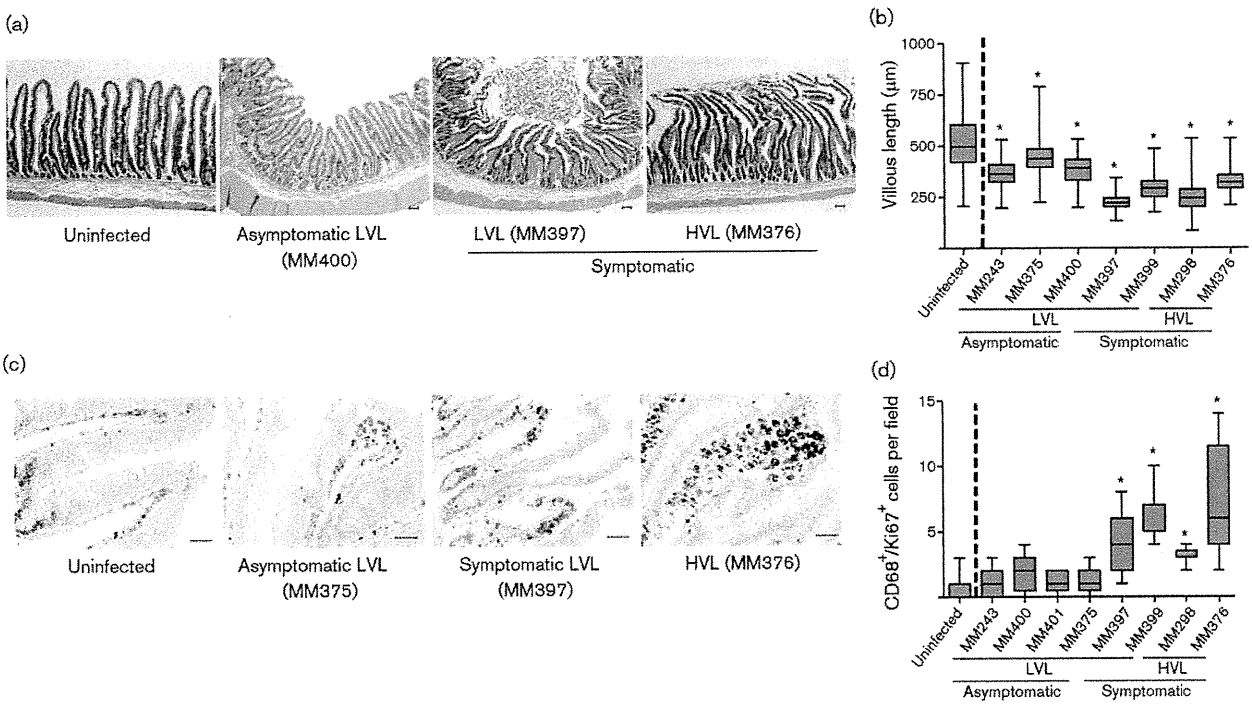

Fig. 3. Villous length in jejunum and counts of activated macrophages in the small intestine at the time of euthanasia in SHIV-KS661-infected rhesus macaques. (a) H&E-stained sections of jejunum of representative uninfected, Asym LVL, Sym LVL and HVL macaques. Bars, 200 μm. (b) Comparison of villous length in uninfected and infected macaques. The lengths of at least 100 villi were measured in each macaque. Statistical analysis was performed using Student's *t*-test for the data from four uninfected and each infected macaque (*, $P<0.0001$). Data for MM299, MM338, MM339 and MM401 were not available. (c) Ki67 and CD68 staining in the small intestine of representative uninfected, Asym LVL, Sym LVL and HVL macaques. Brown staining indicates $Ki67^+$ cells and blue staining indicates $CD68^+$ cells. Bar, 50 μm. (d) Comparison of $CD68^+$ $Ki67^+$ cell counts in uninfected and infected macaques. The numbers of $CD68^+$ $Ki67^+$ cells were enumerated in at least ten fields of the tissues at a magnification of 200×. Statistical analysis was performed using Student's *t*-test for the data from seven uninfected and each infected macaque (*, $P<0.0001$). Data for MM299, MM338 and MM339 were not available.

an LVL. The LVL macaques had much stronger antibody responses than the HVL macaques (Table 1). SHIV-89.6P is easily controlled by the antibody response (Montefiori *et al.*, 1998). SHIV-KS661, which shares its genetic origin with SHIV-89.6P, might be strongly affected by the antibody response. Virus replication during the primary phase clearly occurred later in the intrarectally inoculated macaques than in the intravenously inoculated macaques. Therefore, this delay might contribute to the continuous and strong antibody response in the intrarectally inoculated macaques, consequently resulting in a low viral load in most of the intrarectally inoculated macaques.

The purpose of this study was to elucidate why LVL macaques experience diarrhoea and wasting. A comparison of circulating $CD4^+$ T-cell counts (Fig. 2a) and relative levels of naïve T-cells (Fig. 2b) in LVL macaques did not reveal a substantial difference between Sym LVL (which showed diarrhoea and wasting) and Asym LVL (which were healthy) macaques. The villous length in the intestine also did not affect the level of malignancy of the disease condition, as all infected monkeys showed significant villous atrophy, suggesting a high sensitivity to infection itself. However, Sym LVL and HVL macaques exhibited two findings that Asym LVL macaques did not: (i) $CD4^+$ cell reduction in intestinal and lymphoid tissues (Fig. 2c, d), a hallmark of AIDS; and (ii) abnormal innate immune activation, which was reflected by an increased number of activated macrophages within the intestines (Fig. 3c, d). Ki67 serves as a proliferation marker and proliferation of macrophages may seem unlikely. However, there are some reports about local macrophage proliferation in inflammation sites, indicating the infiltration of activated macrophages associated with tissue damage (Isbel *et al.*, 2001; Norton, 1999). These observations indicated the existence of immunopathological disorders in the intestines not only in HVL macaques but also in Sym LVL macaques.

Many studies have shown positive correlations between the development of AIDS and some characteristic features in

the intestinal tracts of HIV-1-infected humans and pathogenic SIV- or SHIV-infected monkeys: continuous $CD4^+$ T-cell depletion (Brenchley *et al.*, 2004; Ling *et al.*, 2007), abnormal and chronic immune activation (Brenchley *et al.*, 2006; Hazenberg *et al.*, 2003) and enteropathy (Kotler, 2005). Immune activation (as shown by an increased number of intestinal activated macrophages) and intestinal $CD4^+$ cell depletion in Sym LVL macaques strongly suggest the presence of an AIDS-like disease in this subset of animals. Hence, these results suggest that an AIDS-like intestinal disease can occur in LVL macaques despite their low viral load, as well as in HVL macaques.

Some HIV-1-infected patients experience poor recovery of circulating $CD4^+$ T cells, even when their plasma HIV-1 RNA load is suppressed by HAART (Kaufmann *et al.*, 2003; Marchetti *et al.*, 2006; Piketty *et al.*, 1998). These individuals are called immunological non-responders (Marchetti *et al.*, 2006), and have been found to have increased plasma lipopolysaccharide levels, suggesting that bacteria had been translocated from the intestines into the circulation with concomitant activation of T-cell compartments (Marchetti *et al.*, 2006, 2008). Furthermore, some patients who maintain an undetectable or nearly undetectable plasma viral RNA load in the absence of HAART also develop AIDS disease progression (Madec *et al.*, 2005) and have abnormal immune activation and increased plasma lipopolysaccharide levels (Hunt *et al.*, 2008). These observations may indicate that disease progression in a subset of HIV-1-infected individuals is independent of viraemia. Accordingly, the disease progression under conditions of low viral load that we observed in SHIV-KS661-infected macaques can also occur in HIV-1-infected individuals.

Consistent with the fact that intestinal $CD4^+$ cell depletion triggers mucosal immune dysfunction, a notable difference observed between Sym LVL and Asym LVL macaques was the low $CD4^+$ cell frequency in the intestines of the Sym LVL macaques. We propose that the intestinal $CD4^+$ cells in Sym LVL macaques were not able to recover after intestinal $CD4^+$ cell reduction during the early phases of infection. We reported previously that SHIV-KS661 infection of rhesus macaques caused early intestinal $CD4^+$ T-cell depletion (Fukazawa *et al.*, 2008; Miyake *et al.*, 2006). Although we did not examine the macaques during the early phases of infection, the intestinal $CD4^+$ T cells of both Sym LVL and Asym LVL macaques should have been depleted at this time, as even moderately pathogenic SHIV can cause intestinal $CD4^+$ cell reduction during the early phase of infection (Fukazawa *et al.*, 2008). Therefore, the near-normal frequency of intestinal $CD4^+$ cells in Asym LVL macaques would be the result of $CD4^+$ cell recovery after intestinal $CD4^+$ cell reduction during the early phase of infection. In contrast, intestinal $CD4^+$ cells in Sym LVL macaques may be unable to recover, even though virus replication has been controlled. Similarly, intestinal $CD4^+$ cell recovery was found to be important for halting disease progression in SIVmac239-infected rhesus macaques (Ling *et al.*, 2007). Accordingly, one of the important determinants for disease progression in SHIV-KS661-infected macaques may be $CD4^+$ cell recovery in the intestines.

We further hypothesize that this inappropriately low level of $CD4^+$ cells within the intestines of the SHIV-KS661-infected animals (and phenotypically similar humans) is permissive to the excessive activation of resident tissue macrophages. One implication of these studies is that regulatory T-cell subsets of $CD4^+$ cells may be especially vulnerable to this depletion, thus allowing this macrophage activation in view of the well-known role of regulatory T cells in inhibiting innate immune responses (Maloy *et al.*, 2003). This hypothesis will be important to assess in future studies to understand the pathophysiology in the intestines during the chronic phase of HIV-1 infection.

Taken together, the present results suggest that $CD4^+$ cell reduction and enteropathy can occur in SHIV-KS661-infected rhesus macaques even when the viral load is low. The ability or inability to restore intestinal $CD4^+$ cells may be a key factor determining disease progression, irrespective of virus replication levels in the chronic phase of SHIV-KS661 infection. The reason that the recovery of intestinal $CD4^+$ cells is impeded is unknown, although we can speculate on some possibilities such as the co-existence of other infectious microbial agents or impaired T-cell reconstitution caused by damage during thymopoiesis at an early phase of SHIV infection (Motohara *et al.*, 2006). We demonstrated comparable proviral DNA loads in the examined tissues between Sym and Asym LVL macaques, although the $CD4^+$ cell frequencies in the tissues were clearly reduced in Sym LVL macaques. Therefore, the quantity of provirus per CD4 cell in the tissues of Sym LVL macaques is considered to be relatively higher than that of Asym LVL macaques, and low-level replication that may be undetectable in the plasma viral load might be maintained in Sym LVL but not in Asym LVL macaques. Identifying the mechanisms of poor recovery of intestinal $CD4^+$ cells is needed to understand AIDS pathogenesis, because, as stated above, some HIV-1-infected patients have low $CD4^+$ T-cell counts even when viraemia is controlled. One useful approach is comparative and periodical analysis, including cellular immunology data, of the intestinal tract of the same animals from the early to the chronic phases using Sym LVL and Asym LVL macaques in this SHIV infection macaque model.

METHODS

Virus, animals and sample collection. Highly pathogenic SHIV-KS661 is a molecular clone of SHIV-C2/1 (GenBank accession no. AF217181), which was derived through *in vivo* passages of SHIV-89.6 (Shinohara *et al.*, 1999). The virus stock was prepared from the supernatant of virus-infected CEMx174 and M8166 human lymphoid cell lines.

All rhesus macaques used in this study were treated in accordance with the institutional regulations approved by the Committee for

Experimental Use of Non-human Primates in the Institute for Virus Research, Kyoto University, Japan. All macaques were inoculated with 2×10^3 50 % tissue culture infectious dose of SHIV-KS661 measured with CEMx174. The animal ID numbers, infection route and when they were euthanized are provided in Fig. 1(a).

Blood was collected periodically using sodium citrate as an anti-coagulant and examined by flow cytometry and for quantification of plasma viral RNA load. Tissue samples were obtained at the time of euthanasia and were used for quantification of proviral DNA and histopathology.

Determination of plasma viral RNA and proviral DNA loads. The viral loads in plasma and proviral DNA loads in lymphoid and intestinal tissues were determined by quantitative RT-PCR and quantitative PCR, respectively, as described previously (Motohara *et al.*, 2006). DNA samples were extracted directly from frozen tissue sections of each monkey using a DNeasy Tissue kit (Qiagen) according to the manufacturer's protocol.

Determination of antibody titres. Anti-HIV antibody titres were determined using a commercial particle agglutination kit (Serodia-HIV1/2; Fujirebio). Isolated plasma samples were serially diluted and assayed. The end point of the highest dilution giving a positive result was determined as the titre.

Flow cytometry. Flow cytometry was performed as described previously (Motohara *et al.*, 2006). Briefly, $CD4^+$ T cells were analysed by a combination of fluorescein isothiocyanate (FITC)-conjugated anti-monkey CD3 (clone FN-18; BioSource) and phycoerythrin-conjugated anti-human CD4 (clone NU-TH/I; Nichirei), and subsets of naïve and memory $CD4^+$ cells were analysed by a combination of FITC-conjugated anti-human CD95 (clone DX2; BD Pharmingen) and allophycocyanin-conjugated anti-human CD4 (clone L200; BD Pharmingen). $CD95^-$ $CD4^+$ cells were defined as naïve $CD4^+$ T cells and $CD95^+$ $CD4^+$ cells were defined as memory $CD4^+$ T cells. Labelled lymphocytes were examined on a FACSCalibur analyser using CellQuest software (BD Biosciences).

Histology and immunohistochemistry. Tissue samples were fixed in 4 % paraformaldehyde in PBS at 4 °C overnight and embedded in paraffin wax. Sections (4 μm) were dewaxed using xylene, rehydrated through an alcohol gradient, and stained with H&E. The villous length of the jejunum was measured with a micrometer. At least 40 villi from each section were measured.

For immunohistochemistry, sections were rehydrated and processed for 10 min in an autoclave in 10 mM citrate buffer (pH 6.0) to unmask the antigens, sequentially treated with TBS/Tween 20 (TBST) and aqueous hydrogen peroxide, left at 4 °C overnight or at room temperature for 30 min or 1 h for primary antibody reactions, washed with TBST, incubated at room temperature for 1 h with an Envision+ kit (a horseradish peroxidase-labelled anti-mouse immunoglobulin polymer; Dako), visualized using diaminobenzidine (DAB) substrate (Dako) as a chromogen, rinsed in distilled water, counterstained with haematoxylin and analysed by light microscopy (Biozero BZ-8000: Keyence).

For double staining (CD68 and Ki67) of sections, appropriately processed sections were incubated at room temperature for 1 h with unlabelled anti-Ki67 antibody at a dilution of 1:2000, the highly sensitive tyramide amplification step (CSAII; Dako) was performed, the slides were reacted with DAB to visualize the results and incubated with unlabelled anti-CD68 antibody at 4 °C overnight followed by incubation at room temperature for 1 h with Histofine Simple Stain AP (an alkaline phosphatase-labelled anti-mouse immunoglobulin polymer (Nichirei), and the results were visualized with a Blue Alkaline Phosphatase Substrate kit III (Vector Laboratories). Measurements of $CD68^+$ $Ki67^+$ cell counts were performed in ten fields at a magnification of 200 × by light microscopy.

Primary antibodies used in immunohistochemistry were anti-human CD4 (diluted 1:30; clone NCL-CD4; Novacastra Laboratories), anti-SIV Nef (diluted 1:500; FIT Biotech), anti-human CD68 (diluted 1:50; clone KP-1; Dako) and anti-human Ki67 (Ki-S5; Dako).

Statistical analysis. The significance of $CD4^+$ or $CD68^+$ $Ki67^+$ cell frequency measurements and villous length in the jejunum of infected monkeys compared with uninfected monkeys was analysed using an unpaired Student's *t*-test (two-tailed) using GraphPad Prism 4.0E software (Varsity Wave).

ACKNOWLEDGEMENTS

We are grateful to Dr James Raymond for editing the English of this manuscript; to Takahito Kazama, Reii Horiuchi, Noriko Nakajima and Tetsutaro Sata for technical support; to Dr Michael A. Eckhaus for histopathological interpretation; and to Takeshi Kobayashi for critical reading. This work was supported, in part, by Research on HIV/AIDS in Health and Labour Sciences Research Grants from the Ministry of Health, Labour and Welfare, Japan; a Grant-in-Aid for Scientific Research from the Ministry of Education and Science, Japan; a Research Grant for AIDS on Health Sciences focusing on Drug Innovation from the Japan Health Sciences Foundation; and a Program for the Promotion of Fundamental Studies in Health Sciences of the National Institute of Biomedical Innovation (NIBIO) of Japan.

REFERENCES

Anton, P. A., Elliott, J., Poles, M. A., McGowan, I. M., Matud, J., Hultin, L. E., Grovit-Ferbas, K., Mackay, C. R., Chen, I. S. Y. & Giorgi, J. V. (2000). Enhanced levels of functional HIV-1 co-receptors on human mucosal T cells demonstrated using intestinal biopsy tissue. *AIDS* **14**, 1761–1765.

Batman, P. A., Miller, A. R., Forster, S. M., Harris, J. R., Pinching, A. J. & Griffin, G. E. (1989). Jejunal enteropathy associated with human immunodeficiency virus infection: quantitative histology. *J Clin Pathol* **42**, 275–281.

Brenchley, J. M., Schacker, T. W., Ruff, L. E., Price, D. A., Taylor, J. H., Beilman, G. J., Nguyen, P. L., Khoruts, A., Larson, M. & other authors (2004). $CD4^+$ T cell depletion during all stages of HIV disease occurs predominantly in the gastrointestinal tract. *J Exp Med* **200**, 749–759.

Brenchley, J. M., Price, D. A., Schacker, T. W., Asher, T. E., Silvestri, G., Rao, S., Kazzaz, Z., Bornstein, E., Lambotte, O. & other authors (2006). Microbial translocation is a cause of systemic immune activation in chronic HIV infection. *Nat Med* **12**, 1365–1371.

Fackler, O. T., Schafer, M., Schmidt, W., Zippel, T., Heise, W., Schneider, T., Zeitz, M., Riecken, E. O., Mueller-Lantzsch, N. & Ullrich, R. (1998). HIV-1 p24 but not proviral load is increased in the intestinal mucosa compared with the peripheral blood in HIV-infected patients. *AIDS* **12**, 139–146.

Fukazawa, Y., Miyake, A., Ibuki, K., Inaba, K., Saito, N., Motohara, M., Horiuchi, R., Himeno, A., Matsuda, K. & other authors (2008). Small intestine $CD4^+$ T cells are profoundly depleted during acute simian–human immunodeficiency virus infection, regardless of viral pathogenicity. *J Virol* **82**, 6039–6044.

Gibbons, T. & Fuchs, G. J. (2007). Chronic enteropathy: clinical aspects. *Nestle Nutr Workshop Ser Pediatr Program* **59**, 89–101.

Hazenberg, M. D., Otto, S. A., van Benthem, B. H., Roos, M. T., Coutinho, R. A., Lange, J. M., Hamann, D., Prins, M. & Miedema, F.

(2003). Persistent immune activation in HIV-1 infection is associated with progression to AIDS. *AIDS* **17**, 1881–1888.

Hunt, P. W., Brenchley, J., Sinclair, E., McCune, J. M., Roland, M., Page-Shafer, K., Hsue, P., Emu, B., Krone, M. & other authors (2008). Relationship between T cell activation and $CD4^+$ T cell count in HIV-seropositive individuals with undetectable plasma HIV RNA levels in the absence of therapy. *J Infect Dis* **197**, 126–133.

Isbel, N. M., Nikolic-Paterson, D. J., Hill, P. A., Dowling, J. & Atkins, R. C. (2001). Local macrophage proliferation correlates with increased renal M-CSF expression in human glomerulonephritis. *Nephrol Dial Transplant* **16**, 1638–1647.

Kahn, E. (1997). Gastrointestinal manifestations in pediatric AIDS. *Pediatr Pathol Lab Med* **17**, 171–208.

Kaufmann, G. R., Perrin, L., Pantaleo, G., Opravil, M., Furrer, H., Telenti, A., Hirschel, B., Ledergerber, B., Vernazza, P. & other authors (2003). CD4 T-lymphocyte recovery in individuals with advanced HIV-1 infection receiving potent antiretroviral therapy for 4 years: the Swiss HIV Cohort Study. *Arch Intern Med* **163**, 2187–2195.

Kotler, D. P. (2005). HIV infection and the gastrointestinal tract. *AIDS* **19**, 107–117.

Lapenta, C., Boirivant, M., Marini, M., Santini, S. M., Logozzi, M., Viora, M., Belardelli, F. & Fais, S. (1999). Human intestinal lamina propria lymphocytes are naturally permissive to HIV-1 infection. *Eur J Immunol* **29**, 1202–1208.

Ling, B., Veazey, R. S., Hart, M., Lackner, A. A., Kuroda, M., Pahar, B. & Marx, P. A. (2007). Early restoration of mucosal CD4 memory CCR5 T cells in the gut of SIV-infected rhesus predicts long term non-progression. *AIDS* **21**, 2377–2385.

Madec, Y., Boufassa, F., Porter, K. & Meyer, L. (2005). Spontaneous control of viral load and CD4 cell count progression among HIV-1 seroconverters. *AIDS* **19**, 2001–2007.

Maloy, K. J., Salaun, L., Cahill, R., Dougan, G., Saunders, N. J. & Powrie, F. (2003). $CD4^+CD25^+$ T_R cells suppress innate immune pathology through cytokine-dependent mechanisms. *J Exp Med* **197**, 111–119.

Marchetti, G., Gori, A., Casabianca, A., Magnani, M., Franzetti, F., Clerici, M., Perno, C. F., Monforte, A., Galli, M. & Meroni, L. (2006). Comparative analysis of T-cell turnover and homeostatic parameters in HIV-infected patients with discordant immune-virological responses to HAART. *AIDS* **20**, 1727–1736.

Marchetti, G., Bellistri, G. M., Borghi, E., Tincati, C., Ferramosca, S., La Francesca, M., Morace, G., Gori, A. & Monforte, A. D. (2008). Microbial translocation is associated with sustained failure in $CD4^+$ T-cell reconstitution in HIV-infected patients on long-term highly active antiretroviral therapy. *AIDS* **22**, 2035–2038.

Miyake, A., Ibuki, K., Enose, Y., Suzuki, H., Horiuchi, R., Motohara, M., Saito, N., Nakasone, T., Honda, M. & other authors (2006). Rapid dissemination of a pathogenic simian/human immunodeficiency virus to systemic organs and active replication in lymphoid tissues following intrarectal infection. *J Gen Virol* **87**, 1311–1320.

Montefiori, D. C., Reimann, K. A., Wyand, M. S., Manson, K., Lewis, M. G., Collman, R. G., Sodroski, J. G., Bolognesi, D. P. & Letvin, N. L. (1998). Neutralizing antibodies in sera from macaques infected with chimeric simian–human immunodeficiency virus containing the envelope glycoproteins of either a laboratory-adapted variant or a primary isolate of human immunodeficiency virus type 1. *J Virol* **72**, 3427–3431.

Motohara, M., Ibuki, K., Miyake, A., Fukazawa, Y., Inaba, K., Suzuki, H., Masuda, K., Minato, N., Kawamoto, H. & other authors (2006). Impaired T-cell differentiation in the thymus at the early stages of acute pathogenic chimeric simian–human immunodeficiency virus (SHIV) infection in contrast to less pathogenic SHIV infection. *Microbes Infect* **8**, 1539–1549.

Norton, W. T. (1999). Cell reactions following acute brain injury: a review. *Neurochem Res* **24**, 213–218.

Paiardini, M., Frank, I., Pandrea, I., Apetrei, C. & Silvestri, G. (2008). Mucosal immune dysfunction in AIDS pathogenesis. *AIDS Rev* **10**, 36–46.

Piketty, C., Castiel, P., Belec, L., Batisse, D., Si Mohamed, A., Gilquin, J., Gonzalez-Canali, G., Jayle, D., Karmochkine, M. & other authors (1998). Discrepant responses to triple combination antiretroviral therapy in advanced HIV disease. *AIDS* **12**, 745–750.

Sestak, K. (2005). Chronic diarrhea and AIDS: insights into studies with non-human primates. *Curr HIV Res* **3**, 199–205.

Sharpstone, D. & Gazzard, B. (1996). Gastrointestinal manifestations of HIV infection. *Lancet* **348**, 379–383.

Shinohara, K., Sakai, K., Ando, S., Ami, Y., Yoshino, N., Takahashi, E., Someya, K., Suzaki, Y., Nakasone, T. & other authors (1999). A highly pathogenic simian/human immunodeficiency virus with genetic changes in cynomolgus monkey. *J Gen Virol* **80**, 1231–1240.

Smith, P. D., Meng, G., Salazar-Gonzalez, J. F. & Shaw, G. M. (2003). Macrophage HIV-1 infection and the gastrointestinal tract reservoir. *J Leukoc Biol* **74**, 642–649.

Veazey, R. S., DeMaria, M., Chalifoux, L. V., Shvetz, D. E., Pauley, D. R., Knight, H. L., Rosenzweig, M., Johnson, R. P., Desrosiers, R. C. & Lackner, A. A. (1998). Gastrointestinal tract as a major site of $CD4^+$ T cell depletion and viral replication in SIV infection. *Science* **280**, 427–431.

Veazey, R. S., Mansfield, K. G., Tham, I. C., Carville, A. C., Shvetz, D. E., Forand, A. E. & Lackner, A. A. (2000a). Dynamics of CCR5 expression by $CD4^+$ T cells in lymphoid tissues during simian immunodeficiency virus infection. *J Virol* **74**, 11001–11007.

Veazey, R. S., Tham, I. C., Mansfield, K. G., DeMaria, M., Forand, A. E., Shvetz, D. E., Chalifoux, L. V., Sehgal, P. K. & Lackner, A. A. (2000b). Identifying the target cell in primary simian immunodeficiency virus (SIV) infection: highly activated memory $CD4^+$ T cells are rapidly eliminated in early SIV infection in vivo. *J Virol* **74**, 57–64.

Wilcox, C. M. & Saag, M. S. (2008). Gastrointestinal complications of HIV infection: changing priorities in the HAART era. *Gut* **57**, 861–870.

Vaccine 28 (2010) 5377–5385

Contents lists available at ScienceDirect

Vaccine

journal homepage: www.elsevier.com/locate/vaccine

Evaluation of the immune response and protective effects of rhesus macaques vaccinated with biodegradable nanoparticles carrying gp120 of human immunodeficiency virus

Ai Himeno[a], Takami Akagi[b,d], Tomofumi Uto[c,d], Xin Wang[c,d], Masanori Baba[c,d], Kentaro Ibuki[a], Megumi Matsuyama[a], Mariko Horiike[a], Tatsuhiko Igarashi[a], Tomoyuki Miura[a,d,*], Mitsuru Akashi[b,d,**]

[a] Laboratory of Primate Model, Experimental Research Center for Infectious Diseases, Institute for Virus Research, Kyoto University, 53 Shogoinkawaramachi, Sakyo-ku, Kyoto 606-8507, Japan

[b] Department of Applied Chemistry, Graduate School of Engineering, Osaka University, 2-1 Yamadaoka, Suita, Osaka 565-0871, Japan

[c] Division of Antiviral Chemotherapy, Center for Chronic Viral Diseases, Graduate School of Medical and Dental Sciences, Kagoshima University, 8-35-1 Sakuragaoka, Kagoshima 890-8544, Japan

[d] Japan Science and Technology Agency (JST), Core Research for Evolutional Science and Technology (CREST), Saitama 332-0012, Japan

ARTICLE INFO

Article history:
Received 26 January 2010
Received in revised form 6 April 2010
Accepted 15 April 2010
Available online 14 May 2010

Keywords:
HIV vaccine
Biodegradable nanoparticles
Adjuvant

ABSTRACT

We previously reported that biodegradable amphiphilic poly(γ-glutamic acid) nanoparticles (NPs) carrying the recombinant gp120 env protein of the human immunodeficiency virus type 1 (HIV-1) were efficiently taken up by dendritic cells, and induced strong $CD8^+$ T cell responses against the gp120 in mice. To evaluate gp120-carrying NPs (gp120-NPs) as a vaccine candidate for HIV-1 infection, we vaccinated rhesus macaques with these gp120-NPs and examined the immune response and protective efficacy against a challenge inoculation of simian and human immunodeficiency chimeric virus (SHIV). We found that gp120-NP vaccination induced stronger responses for both gp120-specific cellular and humoral immunity than gp120-alone vaccination. After the challenge inoculation with SHIV, however, the peak value of viral RNA in the peripheral blood was higher in the vaccinated groups, especially the gp120-NP vaccinated group, than naive control group. Higher value of viral load was also maintained in gp120-NP vaccinated group. Furthermore, $CD4^+$ T cells from the peripheral blood decreased more in the vaccinated groups than the control group. Thus, induced immune responses against gp120 enclosed in NPs were not effective for protection but, conversely enhanced the infection, although the gp120-NPs showed a stronger induction of immune responses against the vaccinated antigen in rhesus macaques. These results support the importance of determining immune correlate of protective immunity for vaccine development against HIV-1 infection.

1. Introduction

The development of a human immunodeficiency virus type 1 (HIV-1) vaccine is much needed to prevent the continuing spread of the acquired immunodeficiency syndrome (AIDS) pandemic across the world [1]. The use of highly active antiretroviral therapy (HAART) has achieved a reduced death rate due to AIDS. HAART can efficiently suppress virus replication in HIV-1-infected individuals [2]. However, HAART is expensive, and the complete eradication of the virus from infected patients by HAART does not seem possible, suggesting the necessity for long-term treatment. Moreover, the side effects and emergence of drug resistant viruses limit the long-term application of HAART [3]. Thus, an effective, safe and affordable HIV-1 vaccine with prophylactic/therapeutic effects is the most desirable for the eradication of HIV-1 infection.

Vaccination to induce an adaptive immune response is expected for a broad range of infectious diseases. Traditional vaccines are mainly composed of live attenuated viruses or whole inactivated pathogens, and these vaccines often cause many unwanted side effects [4]. With recent advances in biotechnology, new vaccine strategies have been developed using part of the pathogen, such as recombinant/synthetic proteins or peptides, or DNA encoding for these proteins. Subunit vaccines are generally very safe, with well-defined components. However, these antigens are often

* Corresponding author at: Laboratory of Primate Model, Experimental Research Center for Infectious Diseases, Institute for Virus Research, Kyoto University, 53 Shogoinkawaramachi, Sakyo-ku, Kyoto 606-8507, Japan. Tel.: +81 75 751 3984; fax: +81 75 761 9335.

** Corresponding author at: Department of Applied Chemistry, Graduate School of Engineering, Osaka University, 2-1 Yamadaoka, Suita 565-0871, Japan. Tel.: +81 6 6879 7356; fax: +81 6 6879 7359.

E-mail addresses: tmiura@virus.kyoto-u.ac.jp (T. Miura), akashi@chem.eng.osaka-u.ac.jp (M. Akashi).

0264-410X/$ – see front matter © 2010 Elsevier Ltd. All rights reserved.
doi:10.1016/j.vaccine.2010.04.110

poorly immunogenic, and thus require the use of adjuvants or vaccine delivery systems to induce adequate immunity [5–7]. Particulate adjuvants (e.g. micro/nanoparticles, emulsions, ISCOMS, liposomes, virosomes and virus-like particles) have been widely investigated in HIV vaccine delivery systems [8]. Antigen uptake by antigen presenting cells (APCs) is enhanced by the association of these antigens with nano-sized particles. The adjuvant effect of the nanoparticles appears to be largely a consequence of their uptake into the APCs. Dendritic cells (DCs) are highly specialized APCs that can activate naive T cells, and hence initiate primary immune responses. Therefore, the active delivery of antigens to DCs is an important factor for the development of effective vaccines [9,10].

Vaccines to prevent HIV infection have focused on the induction of virus-specific neutralizing antibodies and cytotoxic T lymphocyte (CTL) responses. An important role of neutralizing antibodies for HIV-1 *env* has been demonstrated by the passive transfer of these neutralizing antibodies in animal models. The passive transfer of various human monoclonal antibodies can protect against viral challenge [11–13]. However, it should be noted that for the protection of viral transmission, a high-titer and an enormous quantity of antibodies are needed. Similarly, HIV-1-specific CTL responses have also been associated with the control of HIV-1 infection. The importance of CTL for HIV-1 infection is suggested by the inverse correlation between anti-HIV-1 CTL responses and the virus load in humans [14,15]. In addition, the depletion of $CD8^+$ T cells through the infusion of anti-CD8 antibodies decreases the control of viremia in infected macaques [16,17]. Therefore, recent vaccine approaches have focused on eliciting CTL responses [18]. To solve the problem of the poor immunogenicity of HIV-1 *env*, several candidate adjuvants and delivery systems are currently being investigated in rhesus macaques [19–22]. In fact, the first phase III trial performed using the HIV-1 gp120-based vaccine candidate AIDSVAX from VaxGen was a failure [23]. Varying degrees of protection have been demonstrated in a number of vaccine trials employing the use of a pathogenic simian immunodeficiency virus (SIV) or a chimeric simian/human immunodeficiency virus (SHIV) as the challenge virus [24].

In previous studies, we demonstrated that intranasal immunization with inactivated HIV- or SHIV-capturing polystyrene nanospheres (HIV-NS or SHIV-NS) could induce vaginal anti-HIV-1 gp120 IgA and IgG antibodies in mice [25–27] and macaques, and that SHIV-NS-immunized macaques exhibited partial protection when vaginally and systemically challenged with pathogenic viruses [28]. These results clearly indicated that HIV-1-capturing nanospheres are useful as adjuvant carriers for a prophylactic vaccine against HIV-1 infection. However, both biodegradability and biocompatibility of the adjuvant carriers are required for medical use. Therefore, the development of biodegradable nanoparticles is indispensable for clinical applications [29]. To that end, we have recently prepared protein-loaded biodegradable nanoparticles composed of hydrophobically modified poly(γ-glutamic acid) (γ-PGA) [30–33]. γ-PGA is a naturally occurring water-soluble, biodegradable, edible and non-toxic poly(amino acid)s that is synthesized by certain strains of *Bacillus*. γ-PGA hydrophobic derivatives (γ-hPGA) formed 200 nm-sized nanoparticles (NPs) in water. These protein-encapsulated γ-hPGA NPs were efficiently taken up by immature mouse DCs. These γ-hPGA NPs also had adjuvant activity for DC maturation. Thus, γ-hPGA NPs have significant potential as an antigen carrier and as an adjuvant for DCs [34,35]. Moreover, immunization with HIV-1 gp120- or p24-encapsulated γ-hPGA NPs strongly induced antigen-specific cellular immunity in mice [35–37]. These results suggest that HIV-1-related antigen-carrying γ-hPGA NPs provide a novel delivery system, and function as an adjuvant for vaccination against HIV-1 infection.

In this study, we evaluated the immune responses in macaques after intranasal and subcutaneous immunization with HIV-1 gp120-carrying γ-hPGA NPs (gp120-NPs). Moreover, to determine whether the vaccination by gp120-NPs can enhance the protective effect against pathogenic viruses, the macaques were intravenously challenged with SHIV-KU-2. Here we report the use of nanoparticles as HIV-1 vaccine adjuvants. Our results demonstrated that gp120-NPs have great potential for the induction of HIV-1 gp120-specific cellular and humoral immunity. However, the macaques immunized with gp120-NPs had an augmented viral load. These results may be helpful for the design of HIV-1 vaccines.

2. Materials and methods

2.1. Nanoparticles (NPs)

γ-PGA (number-average molecular weight, $M_n = 3.8 \times 10^5$) was kindly provided by Meiji Seika Co., Ltd., Tokyo, Japan. The synthetic procedures for the γ-hPGA NPs consisting of γ-PGA conjugated with L-phenylalanine ethylester (γ-PGA-*graft*-Phe) and protein-carrying γ-hPGA NPs have been described previously [35,36]. The mean diameter of the γ-hPGA NPs in aqueous solution was measured by a dynamic light scattering (DLS) method using a Zetasizer Nano ZS (Malvern Instruments, UK). The diameter of the NPs was about 200 nm.

2.2. Preparation of gp120-encapsulated γ-hPGA NPs for intranasal vaccination

Recombinant HIV-1 III_B envelope glycoprotein gp120 (Immuno Diagnostics, Woburn, MA) was chosen for the immunization experiments, and encapsulated into the γ-hPGA NPs (gp120-NPs). To prepare the gp120-encapsulated γ-hPGA NP, γ-PGA-*graft*-Phe (10 mg/ml in DMSO) was added to the same volume (500 μl) of 500 μg/ml recombinant gp120 to yield a translucent solution. The resulting solution was centrifuged at 14,000 × *g* for 15 min, repeatedly rinsed to remove the organic solvents, and prepared to a final particle concentration of 20 mg/ml. The gp120 loading content into the NPs was measured by the Lowry method, as previously described [35]. The amount of encapsulated gp120 into the NPs was 10 μg per mg NP.

2.3. Preparation of gp120-surface immobilized γ-hPGA NPs for subcutaneous vaccination

To prepare the gp120-immobilized γ-hPGA NPs, the carboxyl group of the γ-hPGA NPs (10 mg/ml) was first activated by water-soluble carbodiimide (1 mg/ml) for 20 min. The NPs (5 mg/ml) obtained by centrifugation (14,000 × *g* for 15 min) were suspended in 125 μg/ml gp120, and the mixture was incubated at 4 °C for 24 h. After the reaction, the centrifuged NPs were washed twice with PBS. The resulting solution was prepared to a final particle concentration of 20 mg/ml. The amount of gp120 immobilized onto the NPs was 10 μg per mg NP.

2.4. Animals

Nine rhesus macaques (*Macaca mulatta*) of the Indian origin, which spread in Japan, were used in this study. All macaques were serologically negative for simian immunodeficiency virus (SIV) and simian T cell lymphotropic virus type 1. The macaques were housed in P3 level isolators throughout the experimental period. All experiments were carried out in accordance with regulations approved by the Institutional Animal Care and Use Committee of the Institute for virus Research, Kyoto University.

2.5. Vaccination of macaques

Prior to immunization, the macaques were anesthetized by an intramuscular injection of ketamine chloride. Nine macaques were divided into three groups. Three macaques in the gp120-NP group (MM471, MM472 and MM473) were immunized with gp120-carring γ-hPGA NPs, gp120-alone group (MM471, MM472 and MM473) were immunized with gp120 only, and the 3 macaques in the PBS group (MM474, MM475 and MM476) were immunized with phosphate buffered saline (PBS) as a naive control. Each of three macaques was intranasally immunized at 0, 4, and 8 weeks. At each immunization, 0.5 ml of the inoculum (containing 100 μg of gp120 protein encapsulated into or not into 10 mg of NP) was slowly dripped using a pipette tip into both nasal cavities. In addition, these macaques received subcutaneous injections in close proximity to the axillary lymph nodes at 12 and 16 weeks with 1.5 ml of the inoculum containing 300 μg of gp120 immobilized onto or not onto 30 mg of NP.

2.6. Challenge inoculation to macaques

SHIV KU-2 was used in the experiments. SHIV KU-2 is a polyclonal chimeric SHIV generated by in vivo passage of SHIV-4, containing the envelope gene of HIV-1 HXBc2 [38]. The SHIV-KU-2 virus stock for the challenge experiments was produced by culture in rhesus macaque peripheral blood mononuclear cells (PBMCs), and stored in liquid nitrogen until use. The 50% tissue culture infectious dose ($TCID_{50}$) of the virus stock was determined by culture in M8166 cells. At 4 weeks after the last immunization, all nine macaques were intravenously challenged with SHIV-KU-2. For the intravenous challenge, macaques were anesthetized, and then 1×10^5 $TCID_{50}$ of the virus inoculum was used. Blood samples were periodically collected from all macaques. The PBMCs were separated from ACD-A blood by Percoll density centrifugation.

2.7. Quantitative analysis of anti-HIV-1 gp120 IgG and IgA antibodies

HIV-1 gp120-specific IgG and IgA antibody levels in the plasma were measured by an ELISA method. A 96-well microplate (Nunc-Immuno™ Modules, Maxisorp™, Nalga-Nunc, Rochester, NY) was coated with recombinant HIV-1 III_B gp120 (Immuno Diagnostics) at a concentration of 1 μg/ml in 0.1 M Na_2CO_3–$NaHCO_3$ buffer (pH 9.6). The plate was left over night at 4 °C, washed with washing buffer (containing 0.15 M NaCl and 0.05% Tween 20), and treated with a blocking buffer (1% BSA, 1% skim milk in washing buffer) for 2 h at room temperature. To measure the IgG and IgA antibodies, the plasma was 100-fold diluted with blocking buffer, and applied to the plate. The plate was the incubated overnight at 4 °C. After washing with washing buffer, peroxidase-conjugated goat anti-monkey IgG or IgA (Kirkegaard & Perry Laboratories, Gaithersburg, MD) was added to the plate and incubated for 2 h at room temperature. The plate was then washed, and treated with *O*-phenylenediamine dehydrochloride (OPD, Wako Pure Chemical, Osaka, Japan) for 5 min and stopped with 2N H_2SO_4. The specific absorbances were read at 490/690 nm with a microplate reader. The titers of anti-HIV1/2 antibodies in the plasma of all macaques after challenge with SHIV-KU-2 were measured by the particle agglutination (PA) method (Genedia HIV-1/2 mix PA kit, Fujirebio Inc., Tokyo, Japan) following the manufacturer's recommendations.

2.8. Antigen specific proliferation assay

PBMCs from the vaccinated macaques were cultured in triplicate in a 96-well plate (2×10^5 cells/well) with 200 μl of RPMI 1640 medium in the presence of 0.5 μg recombinant HIV-1 III_B gp120 (Immuno Diagnostics) or 1 μg SIV_{mac251} p27 purified native protein (Advanced Biotechnologies, Inc., Columbia, MD) for 72 h. Next, the antigen specific proliferations were measured by BrdU incorporation into the stimulated PBMCs using a cell proliferation ELISA kit (Roche Diagnostic CmbH, Mannheim, Germany) following the manufacturer's recommendations. The stimulation index (SI) for cell activity was calculated using the following formula: stimulation index (SI) = (OD stimulated − blank)/(OD non-stimulated − blank). A SI value above 2.5 was considered as 'antigen-specific' stimulation. Concanavalin A (Con A) was used as a polyclonal stimulator positive control.

2.9. IFN-γ ELISPOT assay

An enzyme-linked immunospot (ELISPOT) assay was performed by stimulating unfractionated PBMCs with recombinant HIV-1 III_B gp120 (Immuno Diagnostics) or SIV_{mac251} p27 purified native protein (Advanced Biotechnologies). MultiScreen 96-Well Plates (Millipore Corporation, Bedford, MA) were coated overnight (100 μl/well) at 37 °C with diluted monoclonal antibody GZ-4 (MABTECH Inc., Mariemont, OH). The plates were then washed 3 times with PBS (−) containing 0.25% Tween 20 (PBS/0.25% Tween 20). The PBMCs were plated in triplicate at 5×10^5/well in 200 μl with either medium alone, 0.5 μg HIV-1 gp120 or 1 μg SIV_{mac251} p27. Following a 72 h incubation at 37 °C, the plates were washed 3 times with PBS/0.25% Tween 20 and incubated for 4 h at 37 °C with a 1:1000 dilution of biotinylated monoclonal antibody 7-B6-1 (MABTECH Inc). Following 3 washes with PBS/0.25% Tween 20, the plates were incubated for 2 h at room temperature with a 1:1000 dilution of streptavidin-alkaline phosphatase (MABTECH Inc). The plate was developed with a BCIP:NBT:0.1 M Tris buffer solution (1:1:10) mixture (Kirkegaard & Perry Laboratories, Gaithersburg, Maryland). Thereafter, the plate was washed 3 times with PBS/0.25% Tween 20, and the reaction stopped by tap water, the plate air dried, and the spots were then read. The mean number of spots from triplicate wells was then calculated for each animal. The data were expressed as the mean number of spots per 10^6 PBMC.

2.10. Quantification of plasma viral RNA loads

Virion-associated SHIV RNA loads in the plasma were measured by real-time reverse transcription (RT)-PCR assay [39]. Briefly, total RNA was prepared from the plasma (140 μl) of each macaque with a QIAamp Viral RNA kit (QIAGEN, Hilden, Germany). RT reactions and PCR were performed by a Platinum qRT-PCR ThermoScript One-Step System (Invitrogen, Carlsbad, CA) using the following primers for the gag region: SIV2-696F (5′-GGA AAT TAC CCA GTA CAA CAA ATAGG-3′), and SIV2-784R (5′-TCT ATC AAT TTT ACC CAGGCA TTT A-3′). A labeled probe, SIV2-731T (5′-Fam-TGTCCA CCT GCC ATT AAG CCC G-Tamra-3′), was used for the detection of the PCR products. These reactions were performed with a Prism 7700 Sequence Detector (Applied Biosystems, Foster City, CA) and analyzed using the manufacturer's software. For each run, a standard curve was generated from dilutions whose copy numbers were known, and the RNA in the plasma samples was quantified based on the standard curve. Under these conditions, the detection limit was 1000 copies/ml.

2.11. Flow cytometric analysis

The frequency of $CD4^+$ T lymphocytes in the whole blood was examined by flow cytometry. Blood samples were immunostained with anti-CD3 (FN-18-FITC; Bio Source, Camarillo, CA), anti-CD4 (L200-APC; Becton-Dickinson, Franklin Lakes, NJ), anti-CD8 (SK1-PerCP; Becton-Dickinson), anti-CD28 (CD28.2-PE;